2013

Micro-Mechanics Based Representative Volume Element Modeling Of Heterogeneous Cementitious Materials

Mohammadmehdi Shahzamanian Sichani
University of Mississippi

MICRO-MECHANICS BASED REPRESENTATIVE VOLUME ELEMENT MODELING OF HETEROGENEOUS CEMENTITIOUS MATERIALS

A Thesis
presented in partial fulfillment of requirements
for the degree of Master of Sceince
in the Department of Mechanical Engineering
The University of Mississippi

by

MOHAMMADMEHDI SHAHZAMANIAN SICHANI

December 2013

ABSTRACT

The current work focuses on evaluation of the effective elastic properties of cementitious materials through a voxel based FEA approach. Voxels are generated for a heterogeneous cementitious material (Type-I cement) consisting of typical volume fractions of various constituent phases from digital microstructures. The microstructure is modeled as a micro-scale representative volume element (RVE) in ABAQUS to generate cubes several tens of microns in dimension and subjected to various prescribed deformation modes to generate the effective elastic tensor of the material. The RVE-calculated elastic properties such as moduli and Poisson's ratio are validated through an asymptotic expansion homogenization (AEH) and compared with rule of mixtures. Both Periodic (PBC) and Kinematic boundary conditions (KBC) are investigated to determine if the elastic properties are invariant due to boundary conditions. In addition the method of "Windowing" was used to assess the randomness of the constituents and to validate how the isotropic elastic properties were determined. The average elastic properties obtained from the displacement based FEA of various locally anisotropic micro-size cubes extracted from an RVE of size 100x100x100 microns showed that the overall RVE response was fully isotropic. The effects of domain size, degree of hydration, kinematic and periodic boundary conditions, domain sampling techniques, local anisotropy, particle size distribution (PSD), and random microstructure on elastic properties are studied.

DEDICATION

This thesis is simply dedicated to my parents.

LIST OF ABERAVIATIONS ANS SYMBOLS

FEA	Finite Element Analysis
FEM	Finite Element Method
RVE	Representative Volume Element
AEH	Asymptotic Expansion Homogenization
KBC	Kinematic Boundary Condition
PBC	Periodic Boundary Condition
PSD	Particle Size Distribution
C-S-H	Calcium Oxide- Silicate Oxide- Hydroxide
ITZ	Interfacial Transition Zone
HD	High Density
LD	Low Density
w/c	Water Cement
2D	Two Dimensional
3D	Three Dimensional

DOH, α	Degree of Hydration
PMD	Periodic Microstructure Domain
STDEV	Standard Deviation
RUS	Resonant Ultrasound Spectroscopy
MM	Multiscale Modeling
F,E,V	Face, Edge and Vertex Respectively Related to PBC formulations
V	Voight
R	Reuss
X	Gel Space Ratio
M	Million
K	Kilo
m	Meter
mm	Millimeter
μm	Micrometer
nm	Nanometer

GPa	Giga Pascal
E	Young Modulus
G	Shear Modulus
K	Bulk Modulus
λ	Lame's First Parameter
υ	Poisson's Ratio
U	Displacement
θ	Angle
L	Length of RVE
ε	Strain
γ	Shear Strain
σ	Stress
D	Elastic Stiffness
C	Individual Components of Stiffness Tensor
a	Anisotropy

V	Volume
U	Total Strain Energy of the RVE
δ	Kronecker Delta
c	Volume Concentration of Inclusion

Subscripts

Unless State Otherwise, the subscripts connote the following meaning when applied with these variables i,j,k,1,2,3,x,y,z,o,c

i,j,k	Related to Directions
1,2,3	Related to Directions
x,y,z	Related to Directions
RVE	Related to Representative Volume Element
o	Related to Initial Values

All other notations and symbols used in formulas are described clearly in the body of thesis.

ACKNOWLEDGEMENTS

First and foremost, I would like to express my deepest gratitude and appreciation to my advisor Dr. Arunachalam Rajendran, chair of the department of mechanical engineering. During these two years he never deprived me from his help and support.

Also, I would like to convey my gratitude to Dr. Tezeswi Tadepalli for his help and collaboration in this thesis.

I would like to acknowledge Mr. Dale Bentz, MCR Division, NIST, for providing guidance on the usage of CEMHYD3D. This study was funded by a grant from the DoD-HBCUs PIRT program and Dr. Joseph Myers serves as the program manager for the US Army Research Office, RTP, NC, USA. The AEH simulations were performed at the DoD Supercomputer Center at Aberdeen Proving Ground, MD. Authors are grateful for the assistance provided by Dr. Brian Hopkins and Mr. Benjamin Pharr at MCSR.

At last, I would like to take this opportunity to express my gratitude to my parents.

TABLE OF CONTENTS

LIST OF TABLES

LIST OF FIGURES

CHAPTER 1

INTRODUCTION

Cementitious materials are composite materials mixed with aggregate and water to form concrete. The cement paste plays the role of a matrix in concrete. Cementitious materials are very complex with properties at several length scales which affect the overall behavior. Cement contains particles such as clinkers and aggregate. When these particles are mixed with water, they undergo hydration, resulting in the formation of new materials. The age of cementitious material is an important parameter in defining its properties, as the properties change when new materials are generated.

Young's modulus and shear modulus are two important mechanical properties in cementitous materials that change over time. Calcium silicate hydrate (CSH) gel is one of the main products of hydration. As the percentage of CSH increases over time, the percentage of water decreases. The C-S-H gel formation between the particles creates a percolation network that can increasingly support the mechanical stresses in the microstructure as hydration proceeds. This phenomenon translates into a corresponding increase in the moduli over time.

The CEMHYD3D suite of programs simulate the evolution of the micro-structure of the cement paste during hydration.. MATLAB software can be used to export the CEMHYD3D output to ABAQUS, resulting in the simulation of microscaled cement paste representative volume element (RVE). This RVE accurately captures the details of all the consistent materials, their size and particle distribution.

The objective of this study is to understand and estimate the effects of heterogeneity on cement strength through microscopic modeling of its deformation behavior.

In order to obtain the young's and shear modulus, boundary conditions need to be imposed on the RVE while applying elementary deformations. Two boundary conditions considered in this study are kinematic boundary condition (KBC) and periodic boundary condition (PBC).

Overall, this study shows that young's and shear modulus increase over time in a cement paste RVE, and there is a negligible difference between the results obtained from imposing KBC and PBC. Moreover, the results obtained from KBC and PBC are compared with another method, asymptotic expansion homogenization (AEH), and KBC and PBC results are in good agreement with the results of AEH. The results show that the heterogeneous cement behaves effectively like an isotropic solid due to the random distribution of the various cement constituents.

In chapter 2, the background of cement will be discussed. Generation of RVE with cemhyd3d and ABAQUS with appropriate and complex boundary conditions will be discussed in chapter 3. Different results of windows and periodic domain size are shown in chapter 5. Finally, conclusion and future work will be presented in chapter 6.

CHAPTER 2

BACKGROUND

Multiscale modeling of materials is an emerging research area to tailor material properties. With the advent of scalable computing capabilities, it is now possible to model a large molecular and representative volume element (RVE) based material systems. The individual elastic properties and density for clinkers, unhydrated and hydrated products are usually estimated through molecular dynamics simulations. These properties are then utilized in the microscopic level RVE simulations. In this paper, we are reporting a methodology for computing the elastic properties of heterogeneous C-S-H (calcium oxide- silicate oxide- hydroxide) based multi-phase cementitious materials. The primary focus of this paper is to predict homogenized properties at macro-levels using micro mechanics based models. This paper focuses on the determination of elastic properties for hydrated cement paste from un-hydrated constituents when small strain quasi-static loading conditions are applied to micro-scale domains.

Typically, Portland cement is often used, in structural concrete along with, sand (fine aggregate), coarse aggregate and solidifies over time because of the addition of water. The tailoring of macroscopic properties (mainly strength) is dependent on its structural applications. The tailored mechanical proprieties for cement-based material are traditionally evaluated at the engineering scale/macroscopic level. However, the strength measured at the macro-level is affected by the chemical phase transformations due to hydration, at the molecular/nano level and the evolution of the microstructure.

Cement is comprised of several constituents that chemically react with the addition of water and uses its covalent bonding mechanisms to bind materials together. When limestone and clay are fused together at 1450 ^{0}C, clinker nodules are formed. The clinker is typically comprised of tricalcium silicate (C_3S), dicalcium silicates (C_2S), tricalcium aluminates (C_3A), calcium ferroaluminates (C_4AF), magnesium oxide (C_4A_3S), calcium silicate hydrate ($C_3S_2H_3$), and, gypsum (CSH_2)[3], shown in Table 1. The tricalcium silicates are responsible for the strength development from 0 to 28 days. The dicalcium silicates are responsible for the strength development after 28 days. The tricalcium aluminates can cause to rapid setting of the cement if not controlled, leading to excessive heating and microcracking. The calcium ferroaluminate is the source of grey color of cement and contributes very slightly to strength gain. The magnesium oxides if not properly minimized can lead to unstable/unsound cements. The fused clinker is then mixed with a small percentage of gypsum (calcium sulfate) and ground down to a fine granular powder that forms cement. The addition of the gypsum to the clinker is used to control the rate of setting and influences the rate of strength development. The C-S-H is the reaction product formed during hydration of cement and is the most important constituent which binds together all constituent material particles.

At least four different length scales (Fig.1) of the constituent material microstructure that affects the properties and loading behavior of concrete have been cited in the literature for the purpose of mechanical analysis [1, 2, 3, and 4].

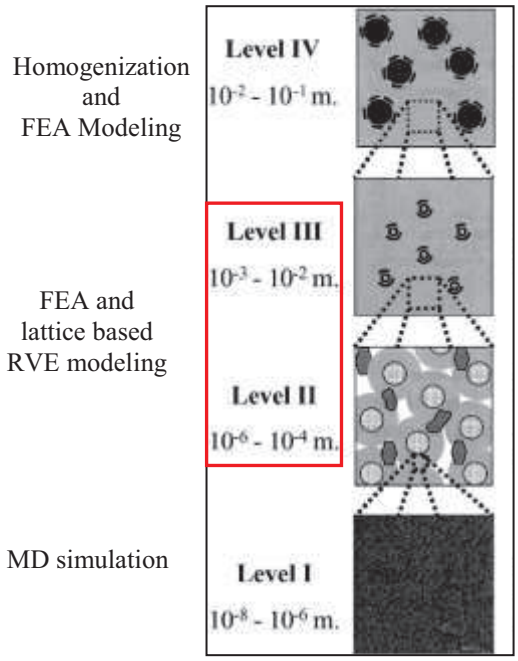

Figure 1. Multilevel micro-structure of cement based materials [2]

These four different configurations for the purposes of mechanical analysis are defined to be:

Level 1 (C-S-H level): At this level, C-S-H exists in two different forms. High density (HD) or low density (LD) C-S-H are present with two distinctive elastic properties [5, 6, 7, 8] due to different packing densities of the same fundamental nanometer scale particles of C-S-H [9].The morphology and volume fraction varies depending on water-cement (w/c) ratio. This level of a characteristic length scale of 10^{-8} – 10^{-6} m is the smallest material length scale that is at present accessible by mechanical testing, i.e., nano-indentation. Research shows that fifty to sixty percent of the hydrated product that is observed in the cement paste is the C-S-H gel [10]. The C-S-H gel is amorphous and its atomic structure is not clearly understood. It is believed that C-S-H gel nanostructure is responsible for controlling the engineering properties such as cohesion and strength of cement paste. In the last twenty years progress has been made towards characterizing the behavior of C-S-H gel [11-17], but substantial work is still needed in the characterization of its complex structure.

Level 2 (Cement paste level): Homogeneous C-S-H with large CH crystals, aluminates, cement clinker inclusions, water. Some capillary porosity may be present depending on the water/cement ratio. Percolation threshold is defined at this scale. The characteristic length scale at this level is 10^{-6} – 10^{-4} m. This scale is the focus of micromechanical modeling in the current study.

Level 3(Mortar level): Sand particles embedded in a homogenous cement matrix paste. Interfacial Transition Zone (ITZ) must be considered as a separate phase [6]. The characteristic length scale at this level is 10^{-3} – 10^{-2} m.

Level 4 (Concrete level): Concrete is a composite material at the structural level and consists of aggregates with ITZ embedded in a homogeneous mortar matrix. The characteristic length scale at this level is 10^{-2} – 10^{-1} m. The homogenization modeling approaches at this scale characterize this level as a three-phase material compound of aggregates embedded in a continuous homogenous mortar matrix and an ITZ.

Starting with the C-S-H colloids, each higher level configuration is built upon an agglomerated configuration of several units of the immediate lower level configurations. This is also known as the hierarchical approach. The mechanical behavior at each level is thus impacted by the clustered configuration of lower length scale constituents. In addition to the traditional material systems, new cementitious/concrete material systems consisting of nano fibers, nano particles, nano foams, etc, have also been considered and have demonstrated to have improved performance for ballistic and shock loading conditions. The presence of these nanomaterial configurations further influences the macro material properties and their behavior under loading conditions [5-9, 17-24]. Since C-S-H colloids are the building blocks of various cementitious materials that can consist of nano fibers, nano particles, nano foams, etc, the present work focuses on determining the fundamental elastic properties of cement using a voxel based FEM approach at the microscale. This approach can provide a basis for the analysis and comparison between the effects of nano-components on material

properties. The ultimate goal is to utilize this approach for designing high strength cement with various additives for infrastructure protection.

CHAPTER 3

METHODOLOGY

3.1. Representative Volume Elements

In order to quantify the role of hydration kinetics on material constituents and the effect of the microstructure in relation to the macro-scale mechanical behavior of cementitious materials; the properties need to be determined at the micro length scales. In recent years there has been an intensive research activity devoted to describing the cementitious materials by computational means [10, 25-40]. At the micro-level the representative volume approach is widely used due to the flexibility and applicability of this method to various physical processes at the micro-scale, such as chemical kinetics, electrical and thermal conductivity, as well as linear and nonlinear elastic properties.

The representative volume element (RVE) is defined as the smallest volume of material that captures the global characteristics of the material. Random results for the overall properties of the material will be obtained if the tested volumes are smaller than this statistically representative subdomain of the microscopic geometry. Such a volume must be sufficiently large to allow a meaningful sampling of the micro-scale stress and strain fields and be sufficiently small for the influence of macroscopic gradients to be negligible and for an analysis of these micro fields to be possible. One of the major objectives of micromechanics is to express in a rigorous form the

continuum quantities associated with an infinitesimal material element as a function of the parameters that characterize its microstructure [41-43]. In general most concrete structures are macroscopic with least dimensions in the order of tens of centimeters or more. The largest aggregates have sizes in the order of a few centimeters. Concrete members are typically designed such that the macroscopic gradients are not significant over dimensions below the centimeter scale. Steep gradients are not generally acceptable in design practice. The 1M and 4M RVEs considered in this study are of the order of hundreds of microns (0.1-0.2 mm) which is small enough for them to be considered infinitesimal.

Alternatively an RVE may be defined as a volume that shows the same overall material properties irrespective of the boundary conditions applied [44, 45]. This definition of an RVE, gives rise to a dependence of the size of the RVE on the physical property considered and on the relative phase contrast. This means that the size of the RVE depends on the mechanical, physical or electrical property being analyzed. As noted by Nemat-Nasser [46], it is the dimension relative to the microstructure essential for a given problem that is important for the size of an RVE. For example, the RVE for thermal conductivity may be different from the RVE for elastic properties [47]. For elastic materials, the RVE exists and one can determine the size of the RVE. However, for other applications, such as the case of softening materials, the RVE may not exist [48].

3.2. Generation of Cementitious RVE

The software package, CEMHYD3D V.3, developed by NIST researchers, was used to simulate the hydration process and formation of the digitally generated micro-structure for a typical Type-I general purpose cement [49]. The software allows creation of a starting 3D microstructure based on a measured geometrical particle size distribution (PSD) (Fig. 2) as well as volume fractions and surface–area fractions of the constituent phases for the cement powder, extracted from 2D composite images of cement at various degrees of hydration.

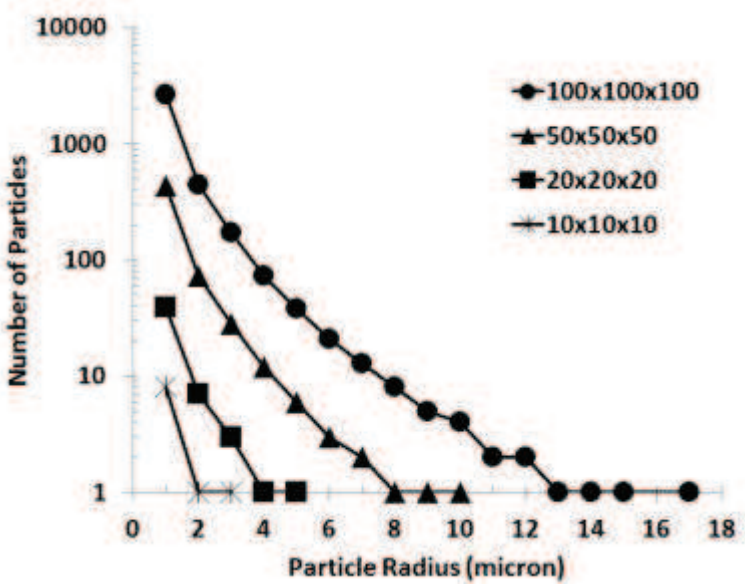

Figure 2. Scaled PSD for initial cement powder in domains of various sizes

To obtain realistic results it is important to establish a suitable domain size to perform the RVE analysis. For this purpose, four different domain sizes 10x10x10 microns (1K), 20x20x20 microns (8K), 50x50x50 microns (125K) and 100x100x100 microns (1M) are considered in this study. To generate a consistent microstructure across various domain sizes, the actual number of particles and pixels are scaled by assuming a constant number-fraction vs particle size (PSD) (Fig.2).

The overall work flow for generating the cement microstructure using CEMHYD3D is shown in Fig. 3. An initial random 3D periodic microstructure is reconstructed with the help of autocorrelation functions and contains typically four cement clinker minerals and forms of calcium sulfate, all as digital spherical particles [49]. Digitized spherical particles of a user-specified PSD are placed into a 3-D computational volume, typically 100 voxels on a side. Each voxel is 1 micron on a side implying that features smaller than this cannot be resolved. However, in the models considered in this study, typical particle sizes range from 1 to 35 microns in diameter, so that most of the factors governing the interphase phenomena can be represented accurately.

Periodic boundaries are employed such that a particle that extends outward through one or more faces of the 3-D microstructure is completed extending inward through the opposite face(s). Such domains will be hence forth referred to as *periodic microstructure domains* (PMD) in this work to distinguish them from *periodic boundary conditions* (PBC) that are applied to both PMD and windows (Section 4). Digitized spherical particles are used to approximate the complex 3-D shapes of actual cement particles. Previous studies [50] have indicated that this approximation is adequate if the actual cement PSD and phase volume and surface fractions are maintained in the 3-D spherical particle image.

Cement hydration products are formed on the grains exposed to water contact and they nucleate in the available volumetric space along with the bound water, and free pore space. In CEMHYD3D, the capillary porosity is composed of the water-filled porosity and the empty porosity. The empty porosity is created due to the ongoing chemical shrinkage that accompanies cement hydration. A schematic of the nano-scale C-S-H phase that forms between the cement clinker grains and binds them together is shown in Fig. 4. The cement products formed from the hydration kinetic reactions are implemented in a rule-based framework similar to cellular

automata. Rules are provided for the dissolution of solid material, diffusion of the generated species, and the various inter-reactions of these species [49].

The RVE approach used in this research assumes a periodic microstructure is forming during hydration which enables homogenization techniques dealing with periodic fields. The volume fractions of major constituents at various stages in the hydration process are shown in Fig. 5 and Figs 6-9 show the process of hydration and particle distributions individually after 3,7,14 and 28 days in whole 1M RVE. These results are obtained by using CEMHYD3D, MATLAB and ABAQUS software. In the next section, the FEA based microscale modeling will be described.

Although the actual hydration time may be determined from the model, the degree of hydration (DOH) is used instead of fitting the parameters to the model cycles [49]. In addition, the PSD dramatically influences the hydration kinetics. Thus the hydrated microstructures of various domain sizes cannot be compared at equal ages and are instead compared after equal degrees of hydration.

Cement microstructure at various DOH up to 0.8 for a water-cement ratio of 0.4 is studied here. The typical Type-I cementitious material considered in this study consists of 17 constituents (Phases) after hydration (Table 1), where E is the Young's Modulus and ν is Poisson's ratio of each corresponding phase.

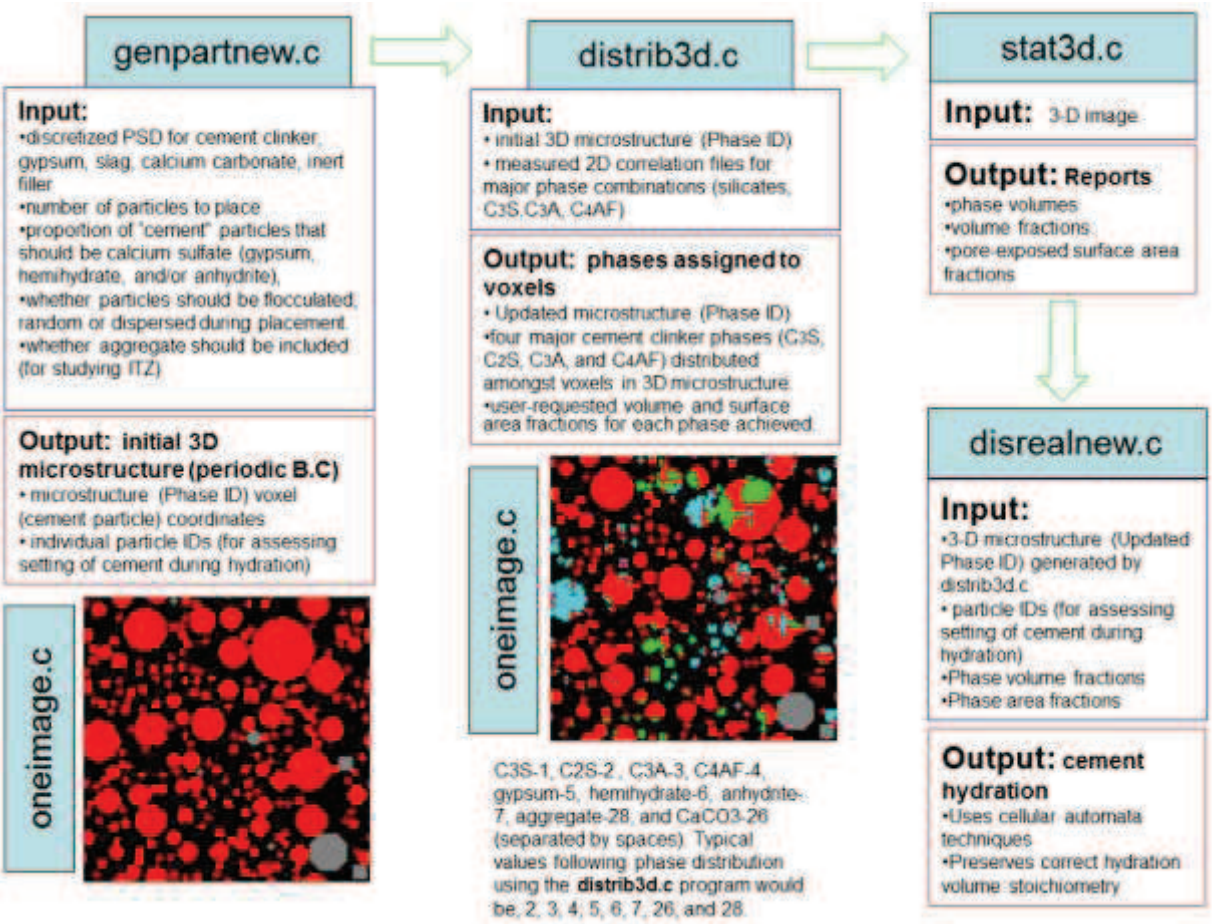

Figure 3. Work flow of the CEMHYD3D program for generation of cement microstructure

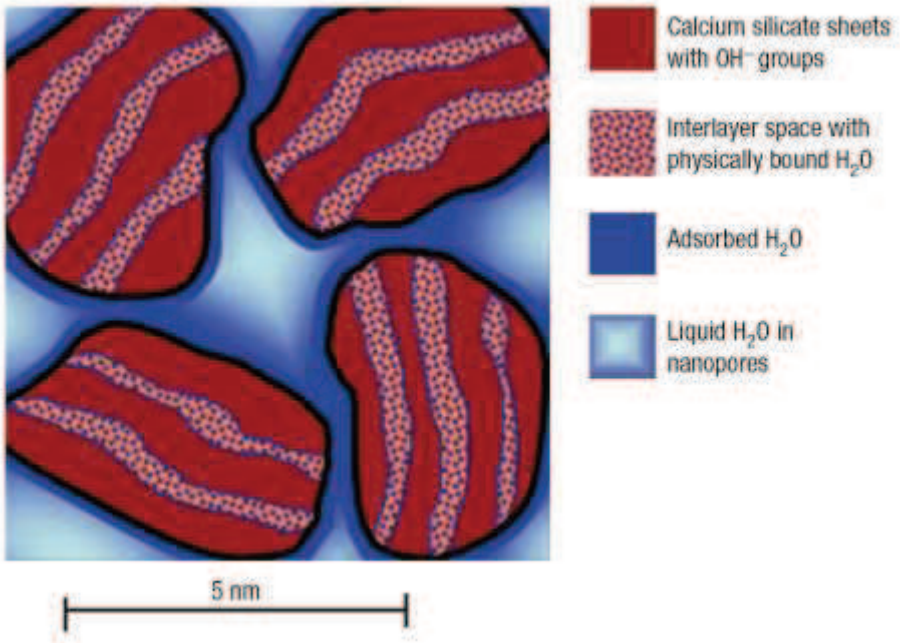

Figure 4. Schematic diagram of the nanoscale C–S–H particles [17]

Table 1. Material properties and volume fractions of constituent phases for a typical Type-I cement (DOH=0.8) [10, 49, 51]

	Phase	**Phase ID**	**Volume Fraction%**	**E (GPa)**	**Poisson's ratio ν**
1	Water Filled Porosity	0	15.2081	0.001	0.499924
2	Tricalcium Silicate (C_3S)	1	4.3537	117.6	0.314
3	Dicalcium Silicate (C_2S)	2	2.3625	117.6	0.314
4	Tricalcium Aluminate (C_3A)	3	1.0822	117.6	0.314
5	Tetracalcium Aluminoferrite (C_4AF)	4	0.8746	117.6	0.314
6	Dihydrate (Gypsum) ($C\bar{S}.H_2$)	5	0.0009	45.7	0.33
7	Hemihydrate ($C\bar{S}.H_{1/2}$)	6	0.0001	62.9	0.30
8	Calcium Hydroxide (CH)	13	16.2595	42.3507	0.324
9	Calcium Silicate Hydrate Gel (CSH)	14	42.3507	22.4	0.25
10	Hydrogarnet (C_3AH_6)	15	4.4651	22.4	0.25
11	Ettringite ($C_6A\bar{S}_3H_{32}$)	16	3.3463	22.4	0.25
12	Iron-rich Stable Ettringite ($ETTRC_4AF$)	17	1.6975	22.4	0.25
13	Monosulfate AFM ($C_4A\bar{S}H_{12}$)	18	5.9672	0.0423	0.324
14	Iron Hydroxide (FH_3)	19	0.4331	22.4	0.25
15	Gypsum Formed from Hemihydrate and Anhydrite (GYPSUMS)	25	0.3200	45.7	0.33
16	ABSGYPS	29	0.0003	45.7	0.33
17	Empty Porosity	45	1.2782	0.001	0.00
Note: According to cement chemistry conventions, C=CaO, S=SiO_2, A=Al_2O_3, F=Fe_2O_3, M=MgO, $\bar{S}$=SO_3, H=H_2O					

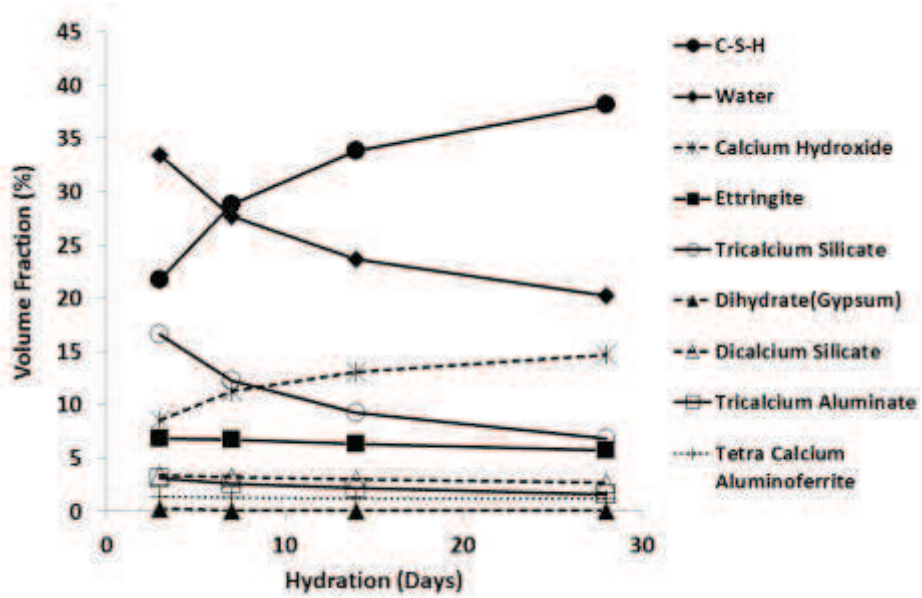

Figure 5. Typical volume fractions of major constituents at various stages of curing

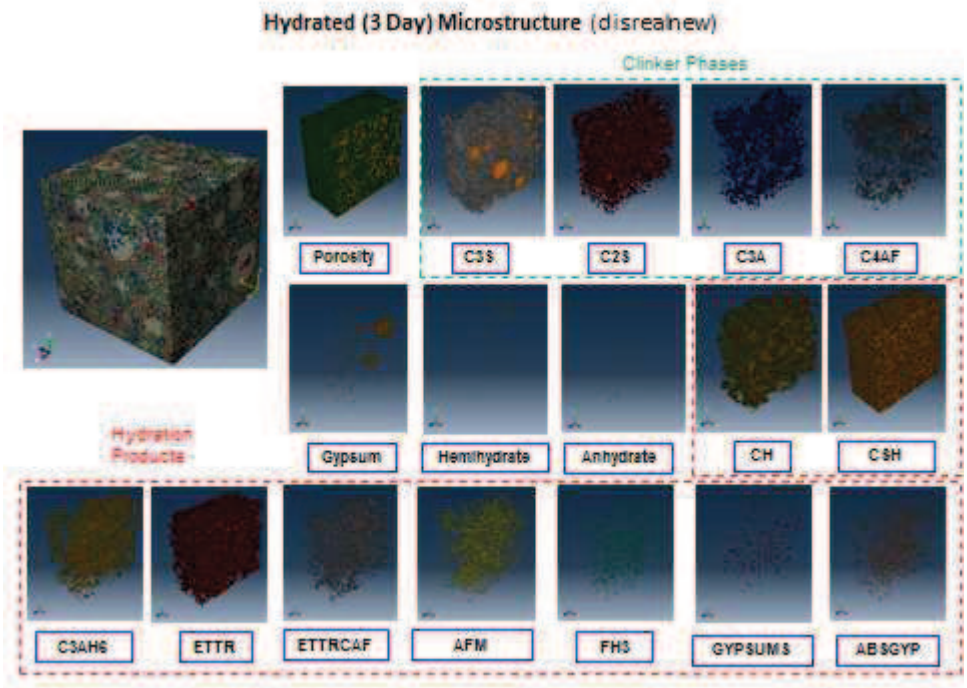

Figure 6. Hydrated Microstructure after 3 Days

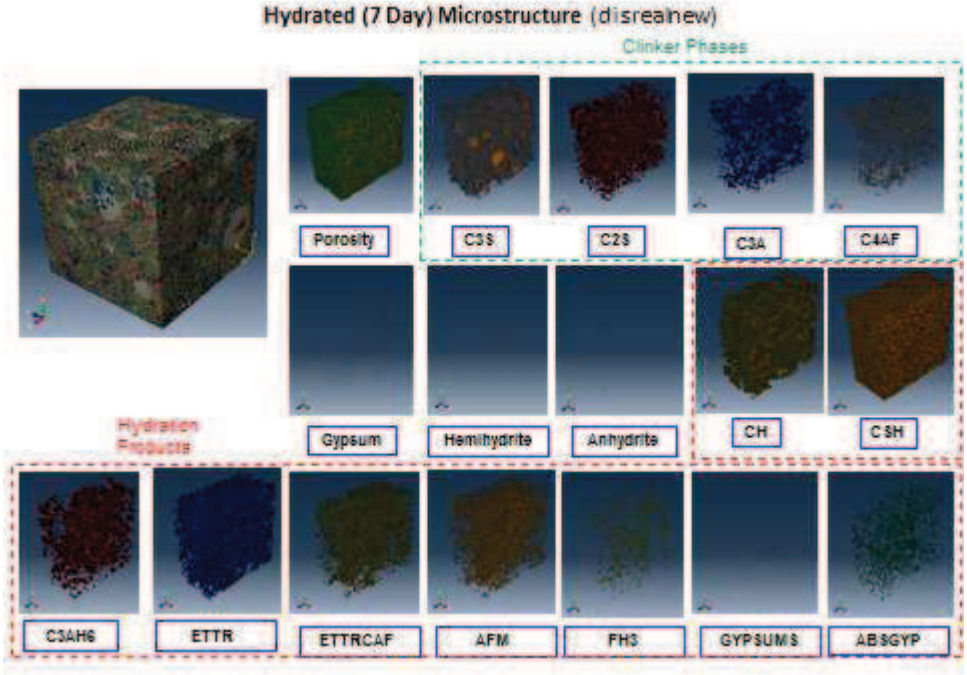

Figure 7. Hydrated Microstructure after 7 Days

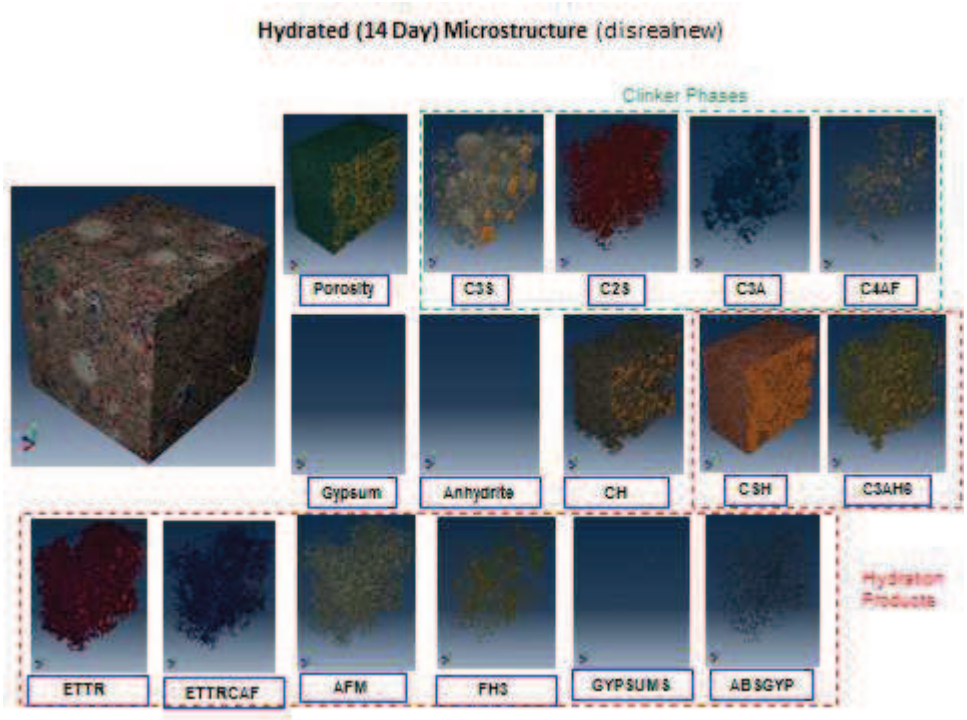

Figure 8. Hydrated Microstructure after 14 Days

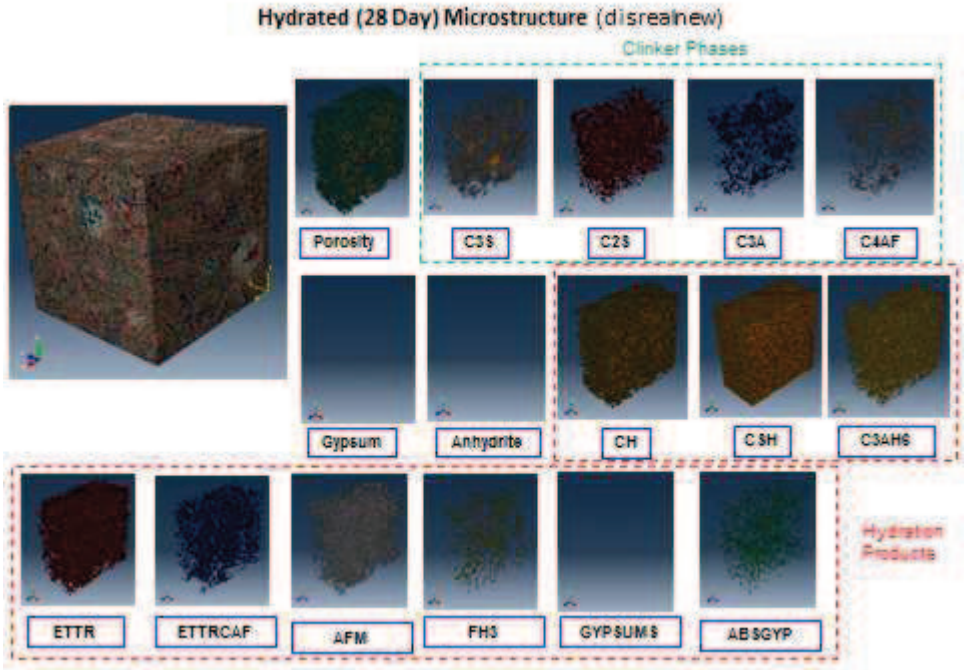

Figure 9. Hydrated Microstructure after 28 Days

3.3. FEA Based Microstructure Modeling

Charmrova [52] focused on the prediction of effective elastic properties using FEA based on a vector microstructural model, specifically applied to early age microstructure. The FEA intense work was mainly to capture the hydration processes accurately, as well as to determine properties of cement at an early age (upto DOH=0.45). In addition the effects of flocculation, water/cement ratio, PSD and number of hydrate clusters, on elastic properties were studied. However, in the present work, the focus is mainly to capture the effects of domain size, degree of hydration, kinematic and periodic boundary conditions, domain sampling techniques, local anisotropy, particle size distribution, and random microstructure on elastic properties are studied. The micro-structure voxel information generated by CEMHYD3D (Fig. 3) is imported into the general purpose ABAQUS® finite element code using an in-house developed Matlab® code and modeled using continuum hexahedral (C3D8) elements to generate domains of various dimensions (Figs.10-11).

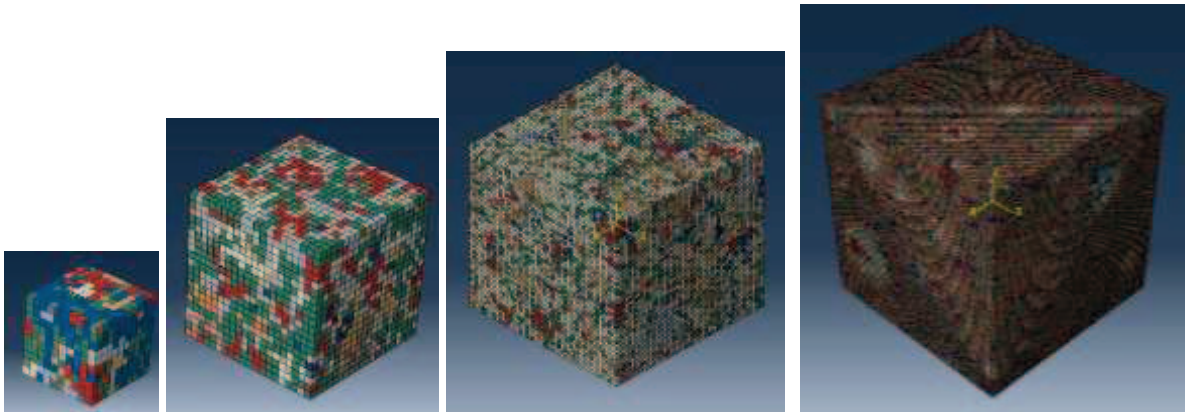

(a) (b) (c) (d)

Figure 10. (a) 1K (b) 8K (c) 125K and (d) 1M FE models of hydrated cement microstructure (PMDs) (not to scale)

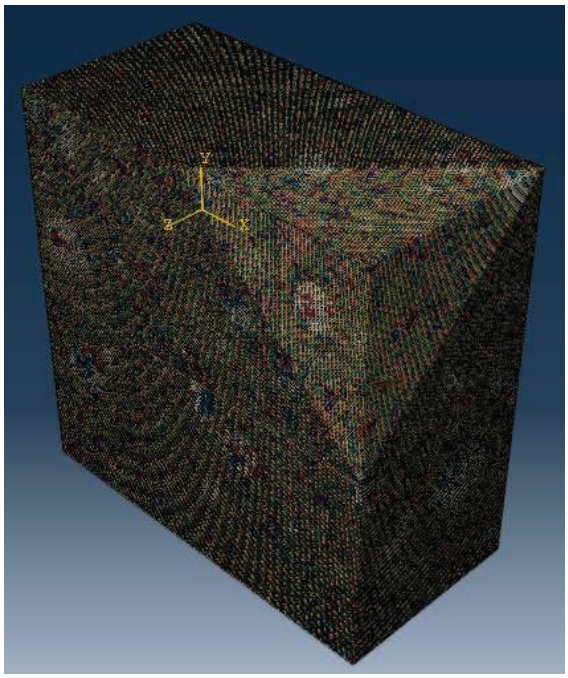

Figure 11. 200x200x100micron (4M) FE model of hydrated cement microstructure (PMD)

3.4. Boundary Conditions

The operational details of applying the appropriate boundary conditions to the microstructure domains are briefly reported in published literature [10, 49, 51-55]. In this section boundary conditions and the issues encountered during modeling are described in sufficient detail to be reproducible using ABAQUS®. The windows and PMDs are subjected to various prescribed tension and shear deformation modes in order to generate the effective elastic tensor of the cementitious material at various scales. Applying the traction/force boundary conditions was found to be non-trivial for the heterogeneous domains since the surface of the cementitious domain also contains porosity which has a modulus of zero. Unfortunately, when a surface traction is applied to a face containing pores on the surface; it results in very large artificial local deformations on the surface of the heterogeneous domain. Previous studies [56] have recommended using a surface layer of elements with a modulus and Poisson's ratio which is the average of all constituent phases. However, this approach may significantly change the relative volume fractions of the various phases, which needs to be preserved for a highly heterogeneous cementitious material. Alternative approaches for applying force boundary conditions are being considered, however, only prescribed displacement (KBC) and periodic boundary conditions (PBC) are described here.

Initially, cubic homogeneous domains of size 1K, 8K, 125K and 1M were subjected to various boundary conditions and the deformations were compared against theoretical values to confirm the absence of any meshing artifacts. Suitable boundary conditions were tested in ABAQUS® for each mode of deformation and the ones that provided an exact match with the theoretical values were used for further study of the heterogeneous periodic domain. In order to generate the elastic tensor of the heterogeneous cementitious material, the periodic domain is subjected to applied displacement boundary conditions as represented in Fig. 12(a) for axial (U_1) and in Fig. 12(b) for pure shear (U_{12}).

In case of uniaxial loading along *x*, *y*, or *z* axes (Fig. 12(a)), the faces with x, y and z =0 have roller BC, such that the nodes on these faces are constrained only in directions perpendicular to the respective faces i.e., for face x-y, displacement U_3=0, for face *x*-*z*, displacement U_2=0 and for face *y*-*z*, displacement U_1=0. The faces with *x*=L_0, *y* = L_0 and z= L_0 are constrained to move as rigid faces such that a large number of nodes (the "coupling" nodes) are constrained to the rigid body motion of the single mid-face node. The nodes in these faces are slaved to the mid-face reference node using kinematic coupling constraints (*KINEMATIC COUPLING). The edge and vertex nodes of the mesh are not constrained. The prescribed traction or displacement loading is applied to the reference node that is coupled to all nodes in the face corresponding to the loading axis. This boundary condition allows the Poisson's effect. In case of pure shear loading (Fig. 12(b)), a uniform traction or displacement is applied on all the nodes of faces with *x*=L_0, and y = L_0. An opposing traction or displacement is applied on all the nodes of faces with *x*=0 and *y*=0. Roller BC (U_3=0) are applied on the face *x*-*y* to constrain against possible rigid body motion of the cube along *z*-axis in the case of smaller domains.

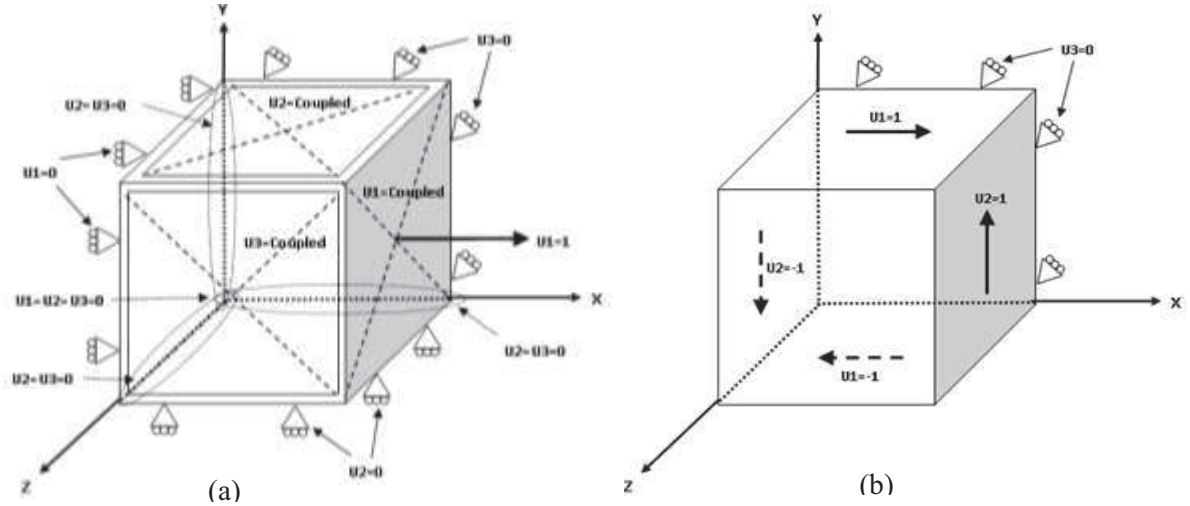

Figure 12. Prescribed Kinematic (KBC) (a) tensile deformation (E1) and (b) pure shear (G12) boundary conditions

Periodic boundary conditions (PBC) are applied to the PMD in order to ensure that the bulk response of the material is simulated without any edge effects (Fig. 13).

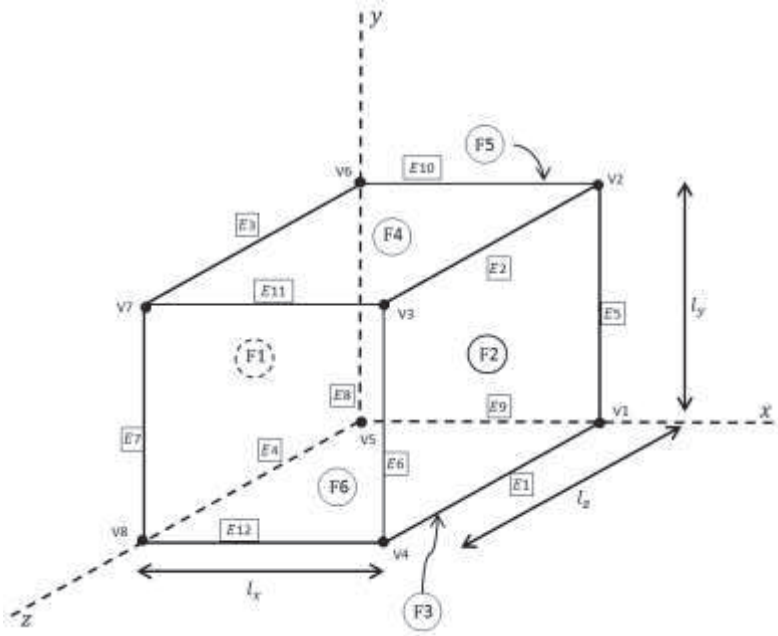

Figure 13. Prescribed Periodic Boundary Conditions (PBC)

As shown below, the equations are formulated such that the differences in displacements between any two opposite faces of the domain are prescribed to be proportional to the applied strain [57].

Nodes on Faces:	**Nodes on Edges:**	**Nodes on Vertices:**
$u_i^{F2} - u_i^{F1} - L_x\varepsilon_{i1} = 0$ $u_i^{F4} - u_i^{F3} - L_y\varepsilon_{i2} = 0$ $u_i^{F6} - u_i^{F5} - L_z\varepsilon_{i3} = 0$	$u_i^{E2} - u_i^{E4} - L_x\varepsilon_{i1} - L_y\varepsilon_{i2} = 0$ $u_i^{E1} - u_i^{E3} - L_x\varepsilon_{i1} + L_y\varepsilon_{i2} = 0$ $u_i^{E6} - u_i^{E8} - L_x\varepsilon_{i1} - L_z\varepsilon_{i3} = 0$ $u_i^{E5} - u_i^{E7} - L_x\varepsilon_{i1} + L_z\varepsilon_{i3} = 0$ $u_i^{E11} - u_i^{E9} - L_y\varepsilon_{i2} - L_z\varepsilon_{i3} = 0$ $u_i^{E10} - u_i^{E12} - L_y\varepsilon_{i2} + L_z\varepsilon_{i3} = 0$	$u_i^{V3} - u_i^{V5} - L_x\varepsilon_{i1} - L_y\varepsilon_{i2} - L_z\varepsilon_{i3} = 0$ $u_i^{V2} - u_i^{V8} - L_x\varepsilon_{i1} - L_y\varepsilon_{i2} + L_z\varepsilon_{i3} = 0$ $u_i^{V7} - u_i^{V1} + L_x\varepsilon_{i1} - L_y\varepsilon_{i2} - L_z\varepsilon_{i3} = 0$ $u_i^{V4} - u_i^{V6} - L_x\varepsilon_{i1} + L_y\varepsilon_{i2} - L_z\varepsilon_{i3} = 0$

Two examples related to uniaxial deformation (E_1) along x-axis and shear deformation (G_{12}) in the x-y plane are illustrated in detail:

Case -1: Applied strain: $\epsilon_{11}\neq 0$. (ϵ_{22}, ϵ_{33}, ϵ_{12}, ϵ_{13} , ϵ_{23} =0) for uniaxial deformation along x-axis.

Nodes on Faces: $\epsilon_{11}\neq 0$, $i=1$	**Nodes on Edges:** $\epsilon_{11}\neq 0$, $i=1$	**Nodes on Vertices:** $\epsilon_{11}\neq 0$, $i=1$
$u_1^{F2} - u_1^{F1} - L_x\varepsilon_{11} = 0$ $u_1^{F4} - u_1^{F3} = 0$ $u_1^{F6} - u_1^{F5} = 0$	$u_1^{E2} - u_1^{E4} - L_x\varepsilon_{11} = 0$ $u_1^{E1} - u_1^{E3} - L_x\varepsilon_{11} = 0$ $u_1^{E6} - u_1^{E8} - L_x\varepsilon_{11} = 0$ $u_1^{E5} - u_1^{E7} - L_x\varepsilon_{11} = 0$ $u_1^{E11} - u_1^{E9} = 0$ $u_1^{E10} - u_1^{E12} = 0$	$u_1^{V3} - u_1^{V5} - L_x\varepsilon_{11} = 0$ $u_1^{V2} - u_1^{V8} - L_x\varepsilon_{11} = 0$ $u_1^{V7} - u_1^{V1} + L_x\varepsilon_{11} = 0$ $u_1^{V4} - u_1^{V6} - L_x\varepsilon_{11} = 0$

Case -2: Applied strain: ϵ_{12} and $\epsilon_{21}\neq 0$. (ϵ_{11}, ϵ_{22}, ϵ_{33}, ϵ_{13}, ϵ_{23} =0) for shear deformation in x-y plane.

Nodes on Faces: $\epsilon_{12}\neq 0$, $i=1$	**Nodes on Edges:** $\epsilon_{12}\neq 0$, $i=1$	**Nodes on Vertices:** $\epsilon_{12}\neq 0$, $i=1$
$u_1^{F2} - u_1^{F1} = 0$ $u_1^{F4} - u_1^{F3} - L_y\varepsilon_{12} = 0$ $u_1^{F6} - u_1^{F5} = 0$	$u_1^{E2} - u_1^{E4} - L_y\varepsilon_{12} = 0$ $u_1^{E1} - u_1^{E3} + L_y\varepsilon_{12} = 0$ $u_1^{E6} - u_1^{E8} = 0$ $u_1^{E5} - u_1^{E7} = 0$ $u_1^{E11} - u_1^{E9} - L_y\varepsilon_{12} = 0$ $u_1^{E10} - u_1^{E12} - L_y\varepsilon_{12} = 0$	$u_1^{V3} - u_1^{V5} - L_y\varepsilon_{12} = 0$ $u_1^{V2} - u_1^{V8} - L_y\varepsilon_{12} = 0$ $u_1^{V7} - u_1^{V1} - L_y\varepsilon_{12} = 0$ $u_1^{V4} - u_1^{V6} + L_y\varepsilon_{12} = 0$
Nodes on Faces: $\epsilon_{21}\neq 0$, $i=2$	**Nodes on Edges:** $\epsilon_{21}\neq 0$, $i=2$	**Nodes on Vertices:** $\epsilon_{21}\neq 0$, $i=2$
$u_2^{F2} - u_2^{F1} - L_x\varepsilon_{21} = 0$ $u_2^{F4} - u_2^{F3} = 0$ $u_2^{F6} - u_2^{F5} = 0$	$u_2^{E2} - u_2^{E4} - L_x\varepsilon_{21} = 0$ $u_2^{E1} - u_2^{E3} - L_x\varepsilon_{21} = 0$ $u_2^{E6} - u_2^{E8} - L_x\varepsilon_{21} = 0$ $u_2^{E5} - u_2^{E7} - L_x\varepsilon_{21} = 0$ $u_2^{E11} - u_2^{E9} = 0$ $u_2^{E10} - u_2^{E12} = 0$	$u_2^{V3} - u_2^{V5} - L_x\varepsilon_{21} = 0$ $u_2^{V2} - u_2^{V8} - L_x\varepsilon_{21} = 0$ $u_2^{V7} - u_2^{V1} + L_x\varepsilon_{21} = 0$ $u_2^{V4} - u_2^{V6} - L_x\varepsilon_{21} = 0$

In ABAQUS® the PBC are enforced using the *EQUATION keyword. The following are the steps in applying PBC on a model:

1. Group the node sets on the faces, edges and vertices of the cube. The *EQUATION keyword allows only those nodes on opposite faces which have matching coordinates. Hence a regular or identical mesh on each the opposing faces are required. In case of irregular mesh, the outermost layers of the RVE geometry need be re-meshed such that this condition is satisfied.
2. The prescribed loading (traction or displacement) is applied on a dummy node situated outside the RVE domain.
3. The mid-nodes on the faces of the RVE need to be constrained in directions orthogonal to prescribed loading to avoid rigid body motion in the cases of uniaxial loading. For example,

in Case-1 described previously, the mid-nodes of faces F3& F4 are assigned boundary condition U3=0 and mid-nodes of faces F5& F6 are assigned boundary condition U2=0.

3.5. Windows

To investigate how the anisotropy due to local microstructure leads to overall isotropic behavior of the agglomerate, the method of windowing is employed. Cubes of size 1K, 8K and 125 K are extracted from 8 locations within the 1M domain which coincide with the gauss quadrature points of a hypothetical C3D8 master element of 1M size. These extracted sub-domains will be referred to as *windows* in subsequent discussions in this study (Fig.14). These are analogous to physical core samples prepared by extraction from a hydrated bulk specimen and are used to sample the 1M domain.

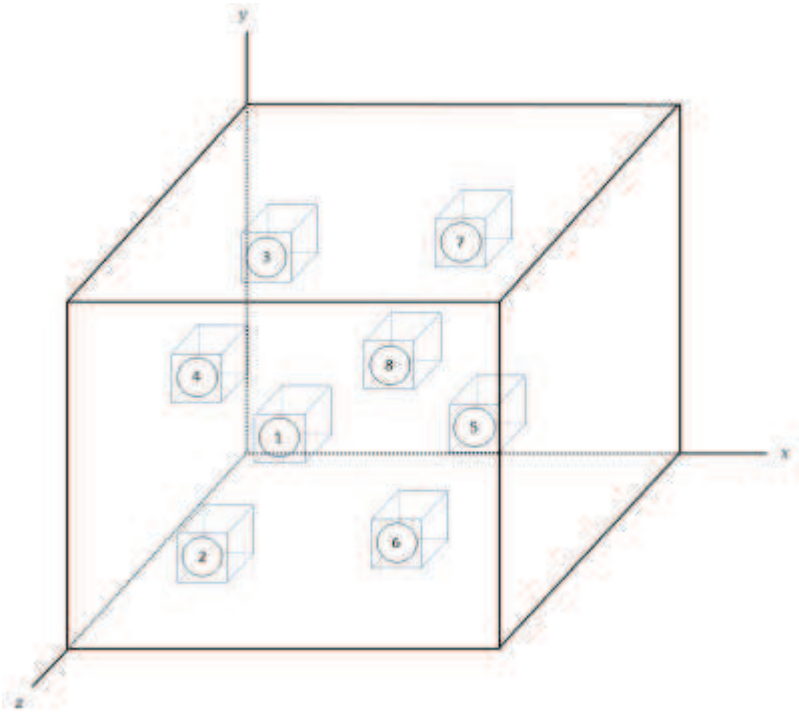

Figure 14. Schematic showing location of windows extracted from the 1M-PMD.

3.6. Homogenization

Homogenization procedures aim at finding a volume element's responses to prescribed mechanical loads (typically far field stresses or far field strains) and to deduce the corresponding overall properties. The most straightforward application of such studies is materials characterization, i.e. simulating the overall material response under simple loading conditions such as uniaxial tensile tests [53]. Modern approaches based on computational homogenization define a microstructural representative volume element that is modeled in full detail. Subsequently, the constitutive equations for the whole object are computed from the representative cell. Several studies have been conducted on obtaining the homogenized or equivalent properties by applying traction or displacement boundary conditions on a periodic domain and the applied boundary conditions are discussed briefly [51,54,55].

The ABAQUS® models consisting of 1 million or more continuum (C3D8) elements are not amenable to being queried for individual element stresses and strains which can then be averaged. Instead the strain energy corresponding to a known applied displacement of the periodic domain is used to determine the corresponding homogenized modulus. Including only non-zero strain terms, the relation for the total strain energy due to deformation (Voigt notation) is given by:

$$U = \frac{1}{2} \cdot \sigma_p^{avg} \cdot \varepsilon_q^{avg} \cdot V_{RVE} \quad (1)$$

Where,

U = total strain energy of the RVE (ABAQUS output)

ε_q^{avg} = average strain (computed from applied displacement), q=1 to 6

V_{RVE} = volume of periodic domain (computed from dimensions of cube)

σ_p^{avg} = average strain (computed from equation 1), p=1 to 6

The homogenized moduli tensor elements are computed by assigning the elastic properties and subjecting the periodic domain to a prescribed pure deformation mode such that only one of the

six independent stresses is non–zero (Figs 10-13). The tensor elements are the ratio of the average stress and strain corresponding to a deformation mode:

$$E_i = \frac{\sigma_i^{avg}}{\epsilon_i^{avg}} \quad \text{and} \quad G_{ij} = \frac{\sigma_i^{avg}}{\epsilon_j^{avg}} \tag{2}$$

Where, E_i = homogeneous modulus corresponding to applied deformation mode (i, j = 1, 2, 3 are not summed indices).

In the case of pure shear deformation (Fig.15), ABAQUS® data output is in terms of engineering shear strain (γ_{xy}) such that:

$$\gamma_{xy} = (\theta_1 + \theta_2) \approx \tan(\theta_1) + \tan(\theta_2) = \left(\frac{\Delta x}{\Delta Y} + \frac{\Delta y}{\Delta X}\right) \tag{3}$$

The tensorial shear strain can be computed as:

$$\varepsilon_{xy} = \frac{1}{2}(\theta_1 + \theta_2) = \frac{1}{2}\left(\frac{\Delta x}{\Delta Y} + \frac{\Delta y}{\Delta X}\right) \tag{4}$$

From (2) the corresponding element of the elastic modulus is computed as:

$$E_i = \frac{2U}{(\varepsilon_i \varepsilon_i) V_{RVE}} \qquad \text{and} \quad G_{ij} = \frac{2U}{(\varepsilon_i \varepsilon_j) V_{RVE}} \tag{5}$$

with no sum on *i*.

For further verification, the present RVE method is compared with asymptotic expansion homogenization (AEH). The AEH method provides an alternate means of estimating the effective elastic properties of general three dimensional microstructures from an RVE [58, 59].

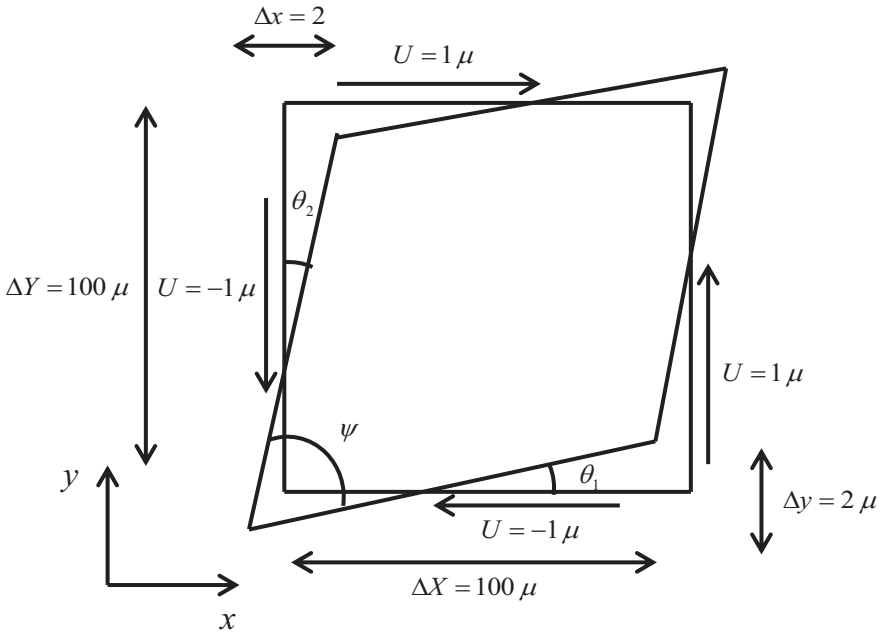

Figure 15. Deformation corresponding to pure shear (G_{12})

For linear elastic inhomogeneous microstructures that exhibit perfectly-periodic homogeneity, an exact estimate of the effective homogeneous elastic properties can be obtained. This involves solving for χ_k^{mn} in Eq. (6):

$$\frac{\partial}{\partial y_j} D_{ijkl}(\mathbf{y}) \frac{\partial \chi_k^{mn}}{\partial y_l} = \frac{\partial}{\partial y_j} D_{ijmn}(\mathbf{y}) \tag{6}$$

subject to periodic boundary conditions on all boundaries of the RVE domain. The summation convention applies to the indices *i, j, k, l, m,* and *n*, which range from 1 to 3. Vector y_i signifies the coordinates of the microstructure RVE, and D_{ijkl} is the elastic stiffness tensor at a point $\mathbf{y}$ in the material. The homogenized linear elastic stiffness tensor, D_{ijmn}^{hom}, is obtained from:

$$D_{ijmn}^{\text{hom}} = \frac{1}{|Y|} \int_Y D_{ijmn}(\mathbf{y}) \left(\delta_{km}\delta_{ln} - \frac{\partial \chi_k^{mn}}{\partial y_l} \right) d^3\mathbf{y} \tag{7}$$

which produces a general estimate of all 81 terms of the anisotropic elastic stiffness tensor. Under symmetries imposed by the geometry of the microstructure, D_{ijmn}^{hom} will possess all appropriate symmetries as well. Thus, the number of terms in D_{ijmn}^{hom} can be reduced in the standard way through symmetry arguments associated with, for instance, orthotropic linear elasticity.

CHAPTER 4

RESULTS

4.1. RVE Deformation in ABAQUS Simulation

This subsection shows RVE deformation due to imposing KBC by ABAQUS simulation. As it was mentioned in section 3.4, KBC is one of the imposed boundary conditions to determine the effective young's and shear modulus. Imposing of KBC has been described in details previously in this thesis. Figs 16 and 17 show the deformation of 1M RVE after imposing KBC for the cases of E_{11} and E_{12}, respectively.

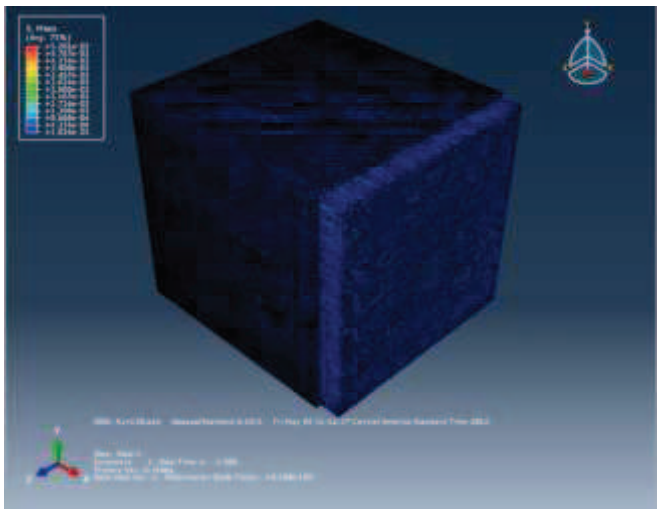

Figure 16 Deformation of 1M RVE due to imposing KBC for the case of E_{11}

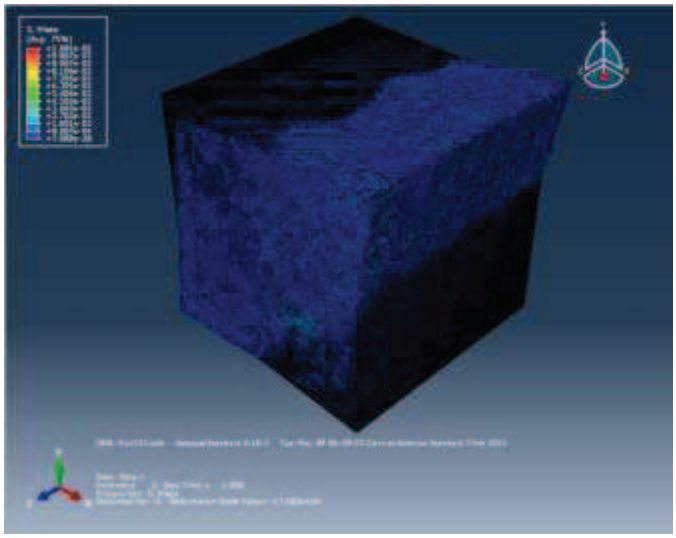

Figure 17 Deformation of 1M RVE due to imposing KBC for the case of E_{12}

Figs 18 and 19 show the deformation of 4M RVE due to imposing KBC for the cases of E_{11} and E_{12}, respectively.

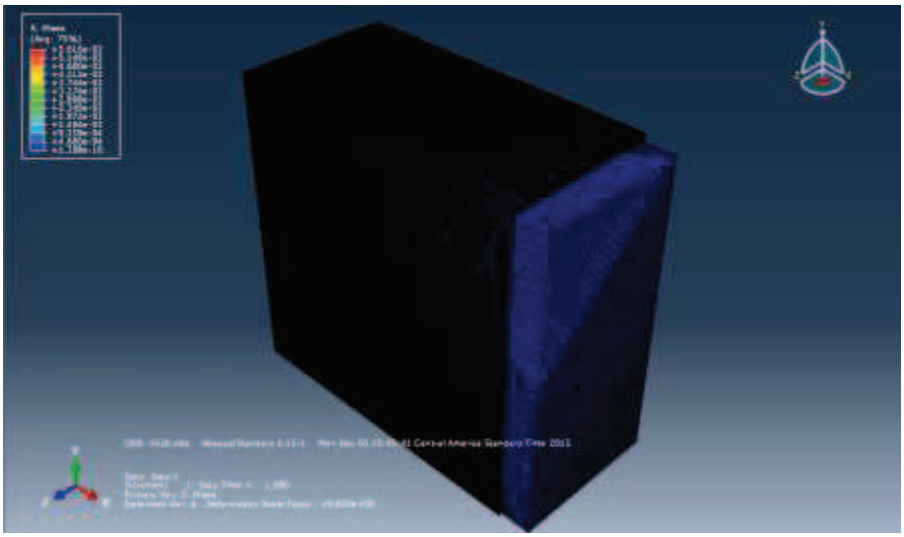

Figure 18 Deformation of 4M RVE due to imposing KBC for the case of E_{11}

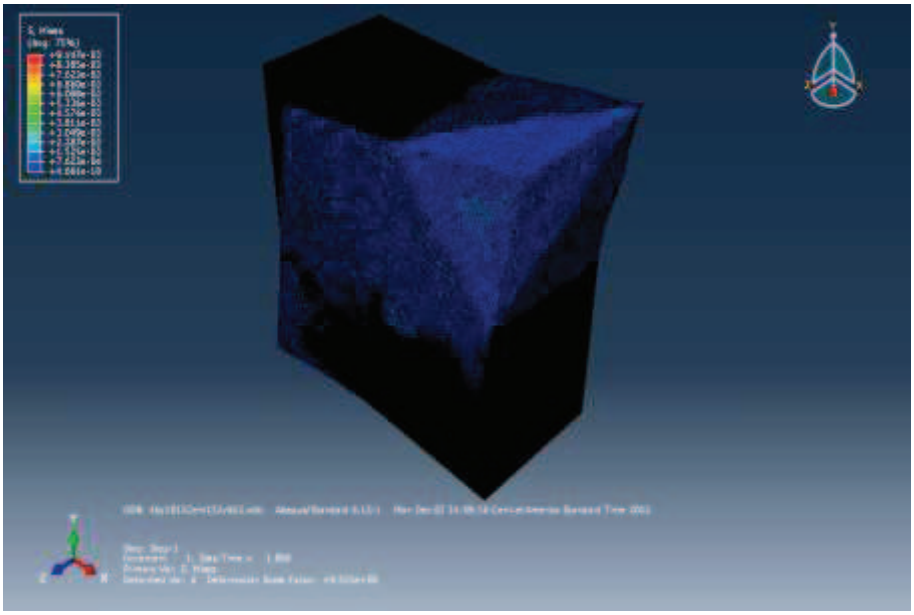

Figure 19 Deformation of 4M RVE due to imposing KBC for the case of E_{12}

Also, deformation modes and corresponding elastic properties of the heterogeneous cementitious 1 Million elements RVE due to imposing KBC are shown in Fig 20.

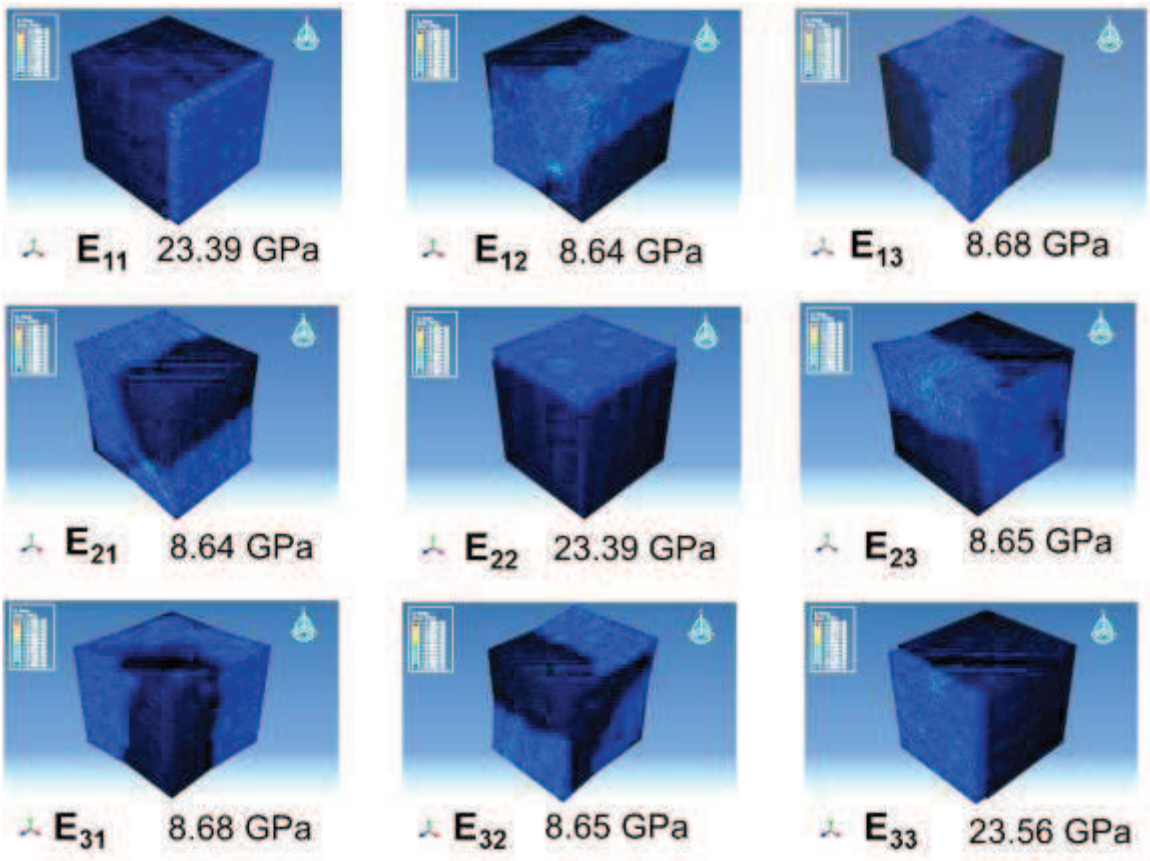

Figure 20. Deformation modes for a 1M RVE (28 Days) for the case of KBC

It can be seen from Fig 20 that cementitious RVE created by CEMHYD3D behaves almost as an isotropic material. It can be observed that RVE is not exactly isotropic and for this reason, anisotropy will be discussed in section 4.2.1.

4.2. Microstructure Based homogenization

4.2.1. Periodic Microstructure Domain (PMD)

In order to study the effect of domain size on elastic properties, PMDs of various sizes: 1K, 8K, 125K and 1M are generated in CEMHYD3D. The input particle size distribution (PSD) is scaled (Fig. 2) in order to keep the relative volume fractions of various constituents in smaller domains similar to those in the 1M PMD. The microstructure of each PMD is captured at various degrees of hydration (DOH =0.3, 0.5 or 0.8) in order to study the evolution of elastic properties of the cement.

As expected, the volume fractions (DOH=0.8) of constituents in PMDs of sizes 8K, 125K and 1M are found to be consistent within domains of the same size and vary only slightly with size as shown in Fig. 21. In domains smaller than 8K, the volume fractions of various constituent phases cannot be maintained due to the low number of particles. In case of the 1K domain the volume fractions of individual constituents become unrealistic. A significant increase is observed in the volume fraction of C-S-H as the domain size increases from 1 K to 8K. This may be due to the fact that C-S-H forms on the active surfaces. Since there are only a few particles, the corresponding ratio of active surfaces to domain volume is relatively less compared to PMDs of size 8K and larger, which have a smoother PSD (Fig. 2). This shows that the hydration kinetics is highly sensitive to PSD. However, beyond 8K, the volume fractions become independent of the domain size.

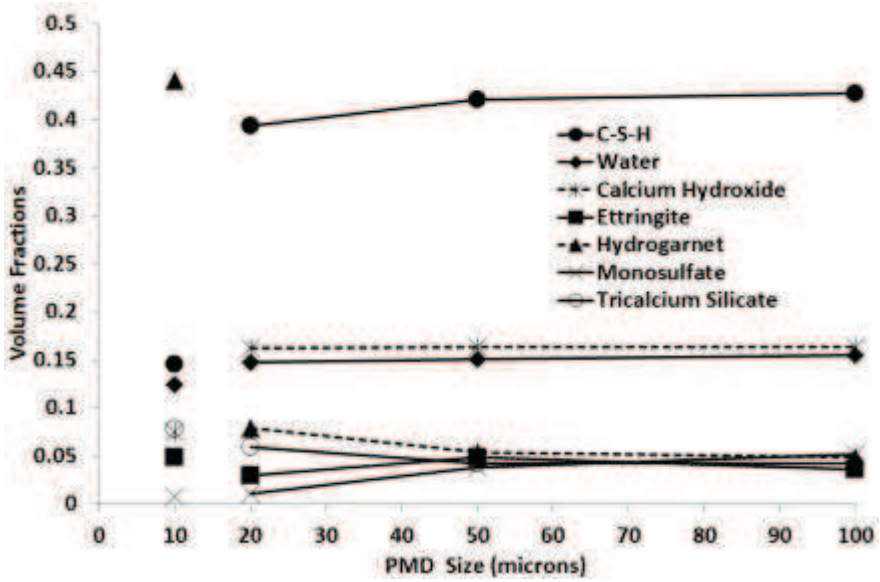

Figure 21. Volume fractions of major phases for 1K, 8K, 125K and 1M PMDs

The effect of spatial distribution of constituents on the elastic properties is studied by generating several instances of the 1M PMD with random spatial distribution of particles within the volume of each domain, while keeping the volume fractions and PSD constant. These instances are subjected to various axial and shear deformation modes in order to determine

corresponding elements of the elastic tensor. Figs. 22(a)-(b) show the cumulative average values of principal and shear moduli of the 1M-PMD for various instances normalized to their respective average. It is seen that spatial distribution of constituent phases has little effect on global elastic properties of the domain.

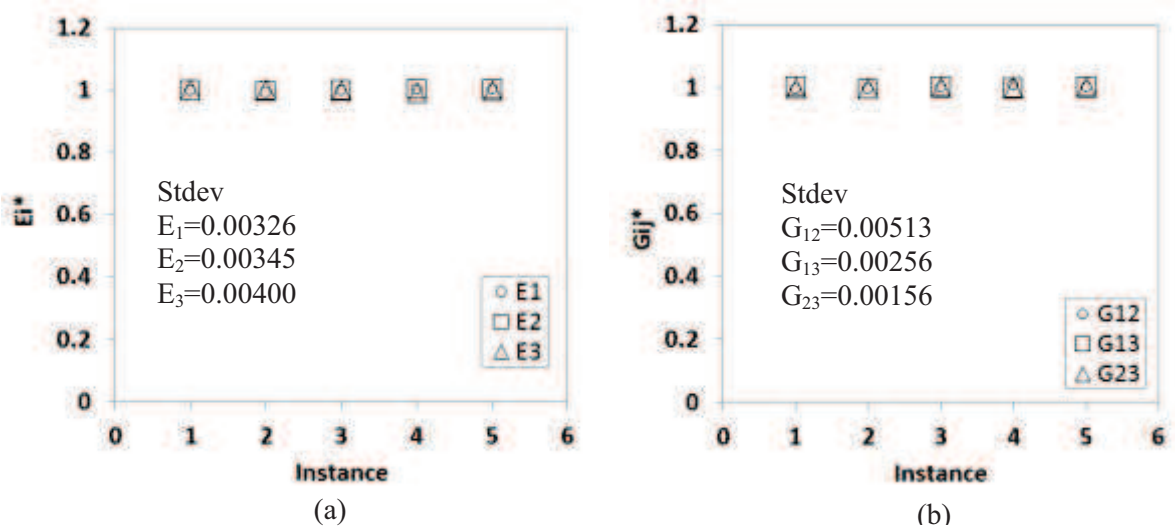

Figure 22. Variation of (a) principal and (b) shear moduli (KBC) in 1M- PMD for various instances normalized to their respective average

The elastic tensor (Voigt notation) for an isotropic material is given by:

$$\begin{Bmatrix}\sigma_1\\ \sigma_2\\ \sigma_3\\ \sigma_4\\ \sigma_5\\ \sigma_6\end{Bmatrix} = \begin{bmatrix} C_{11} & C_{12} & C_{13} & 0 & 0 & 0\\ C_{12} & C_{22} & C_{23} & 0 & 0 & 0\\ C_{13} & C_{23} & C_{33} & 0 & 0 & 0\\ 0 & 0 & 0 & C_{44} & 0 & 0\\ 0 & 0 & 0 & 0 & C_{55} & 0\\ 0 & 0 & 0 & 0 & 0 & C_{66}\end{bmatrix} \begin{Bmatrix}\varepsilon_1\\ \varepsilon_2\\ \varepsilon_3\\ \varepsilon_4\\ \varepsilon_5\\ \varepsilon_6\end{Bmatrix} \tag{8}$$

Where the individual components of the stiffness tensor are given by:

$$C_{11} = -\frac{E_1(1-\nu_{23}\nu_{32})}{\Delta} \qquad C_{12} = -\frac{E_1(\nu_{21}+\nu_{23}\nu_{31})}{\Delta} \qquad C_{13} = -\frac{E_1(\nu_{31}+\nu_{21}\nu_{32})}{\Delta}$$

$$C_{21} = -\frac{E_2(\nu_{12}+\nu_{13}\nu_{32})}{\Delta} \qquad C_{22} = -\frac{E_2(1-\nu_{13}\nu_{31})}{\Delta} \qquad C_{23} = -\frac{E_2(\nu_{32}+\nu_{12}\nu_{31})}{\Delta} \tag{9}$$

$$C_{31} = -\frac{E_3(\nu_{13}+\nu_{12}\nu_{23})}{\Delta} \qquad C_{32} = -\frac{E_3(\nu_{23}+\nu_{13}\nu_{21})}{\Delta} \qquad C_{33} = -\frac{E_3(1-\nu_{12}\nu_{21})}{\Delta}$$

$$C_{44} = G_{12} \qquad C_{55} = G_{13} \qquad C_{66} = G_{23}$$

where, $\Delta = \nu_{12}\nu_{21} + \nu_{13}\nu_{31}\nu_{23}\nu_{32} + \nu_{12}\nu_{23}\nu_{31} + \nu_{13}\nu_{21}\nu_{32} - 1$.

To quantify the anisotropy more precisely, the following parameters were described by Kanit [60]:

$$a = \frac{2Y_{44}}{Y_{11} - Y_{12}} \tag{10}$$

Where,

$$Y_{44} = \frac{C_{44}+C_{55}+C_{66}}{3}, Y_{11} = \frac{C_{11}+C_{22}+C_{33}}{3}, Y_{12} = \frac{C_{12}+C_{23}+C_{13}}{3},$$

The coefficient *a* is equal to 1 if the elastic behavior is perfectly isotropic.

Further the effective engineering constants for an isotropic material can be computed as:

$$Y_{11} = C_1 \;\; ; \; Y_{12} = C_2 \;\; ; \tag{11}$$

$$\lambda = C_2, G = Y_{44}, K = \lambda + \frac{2}{3}G, \quad \nu = \frac{\lambda}{2(\lambda+G)}, E = \frac{G(3\lambda+2G)}{\lambda+G}$$

Note that in Eq.(11) G is defined as Y_{44} instead of $\frac{C_1-C_2}{2}$. In a fully isotropic material (a=1) these values should be identical. However, they may differ depending on the degree of anisotropy in the material. In all KBC cases mentioned below, a total of six pure axial (E_i) and shear deformation (G_{ij}) cases are analyzed and results are summarized in Table 2 and Figs. 23-24. The orthotropic elastic matrix obtained by applying KBC to a 1M-PMD at a DOH of 0.8 using ABAQUS is given as follows:

$$\begin{Bmatrix} \sigma_{11} \\ \sigma_{22} \\ \sigma_{33} \\ \sigma_{12} \\ \sigma_{13} \\ \sigma_{23} \end{Bmatrix} = \begin{bmatrix} 36.1157 & 17.9572 & 17.7946 & 0 & 0 & 0 \\ 18.1901 & 36.3073 & 18.0311 & 0 & 0 & 0 \\ 18.3897 & 18.3948 & 36.4331 & 0 & 0 & 0 \\ 0 & 0 & 0 & 9.0690 & 0 & 0 \\ 0 & 0 & 0 & 0 & 9.0920 & 0 \\ 0 & 0 & 0 & 0 & 0 & 9.0790 \end{bmatrix} \begin{Bmatrix} \varepsilon_{11} \\ \varepsilon_{22} \\ \varepsilon_{33} \\ \varepsilon_{12} \\ \varepsilon_{13} \\ \varepsilon_{23} \end{Bmatrix}$$

Table 2. Effective bulk properties obtained from elastic tensors by applying KBC to PMDs assuming orthotropic symmetry

Domain Size (microns)	DOH	λ (GPa)	G (GPa)	K (GPa)	E (GPa)	ν	a
100x100x100	0.8	18.1211	9.08	24.1744	24.209	0.3331	0.9892
100x100x100	0.5	24.4610	7.613	29.5364	21.032	0.3813	0.9517
100x100x100	0.3	37.7033	5.714	41.5126	16.39	0.4342	0.8854
50x50x50	0.8	18.2599	9.05	24.2933	24.151	0.3343	0.9847
20x20x20	0.8	22.4614	8.917	28.4061	24.217	0.3579	1.0

In the above cases where KBC was applied, the elastic tensor was found to be effectively isotropic. This isotropic behavior is assumed to hold in cases when PBC is applied as well. Hence only two deformation cases corresponding to pure extension (E_1) and pure shear (G_{12}) are required to populate the elastic tensor and obtain the overall effective bulk properties. Since the microstructure and domain size are identical, effective Poisson's ratios obtained from the corresponding KBC cases (Table 2) are used to generate the elastic tensor in this study. This enables efficient computation of the elastic tensor since the PBC cases require significantly larger computational resources. The various trends observed in this analysis are summarized in Table 3 and Figs. 23-24.

Table 3. Effective bulk properties obtained from elastic tensors by applying PBC to PMDs

Domain Size (microns)	**DOH**	**λ (GPa)**	**G (GPa)**	**K (GPa)**	**E (GPa)**	**ν**	**a**
100x100x100	0.8	15.5048	9.1520	21.6061	24.0590	0.3144	0.9979
100x100x100	0.5	15.2035	7.763	20.3789	20.6650	0.3310	0.9942
100x100x100	0.3	12.7297	5.8840	16.6524	15.7920	0.3419	0.9949
50x50x50	0.8	15.3334	9.1540	21.4360	24.0400	0.3131	0.9976
20x20x20	0.8	17.1366	9.1030	23.2053	24.1510	0.3265	1.0

The full anisotropic stiffness matrix for typical cement 1M- PMD (DOH= 0.8) obtained using AEH [58] is:

$$\begin{Bmatrix} \sigma_{11} \\ \sigma_{22} \\ \sigma_{33} \\ \sigma_{12} \\ \sigma_{13} \\ \sigma_{23} \end{Bmatrix} = \begin{bmatrix} 30.6136 & 11.1675 & 11.1704 & 0.0014 & 0.0051 & 0.0329 \\ 11.1675 & 30.6653 & 11.1547 & 0.0178 & -0.006 & 0.0059 \\ 11.1704 & 11.1547 & 30.7280 & 0.0153 & -0.0228 & 0.0504 \\ 0.0014 & 0.0178 & 0.0153 & 9.3531 & 0.014 & -0.0014 \\ 0.0051 & -0.0060 & -0.0228 & 0.014 & 9.3426 & 0.0175 \\ 0.0329 & 0.0059 & 0.0504 & -0.0014 & 0.0175 & 9.3631 \end{bmatrix} \begin{Bmatrix} \varepsilon_{11} \\ \varepsilon_{22} \\ \varepsilon_{33} \\ \varepsilon_{12} \\ \varepsilon_{13} \\ \varepsilon_{23} \end{Bmatrix}$$

Table 4. Effective bulk properties obtained from elastic tensors by applying AEH to various PMDs (DOH=0.8)

Domain Size (microns)	DOH	λ (GPa)	G (GPa)	K (GPa)	E (GPa)	ν	a
100x100x100	0.8	16.5834	9.3550	22.82	24.6910	0.3197	0.9590
100x100x100	0.5	18.9851	8.1146	24.3948	21.9140	0.3503	0.9357
100x100x100	0.3	20.3734	6.3953	24.6369	17.6580	0.3805	0.9182
50x50x50	0.8	16.9219	9.3370	23.1466	24.6910	0.3222	0.9560
20x20x20	0.8	18.3961	9.3200	24.6095	24.8260	0.3319	0.9470

The strength and cohesion of cement paste are controlled by the formation of C-S-H. As the hydration of the cement paste proceeds, the C-S-H gel formation results in the reduction of free water content in the pores which reduces the effective bulk modulus (K) and Poisson's ratio as shown in Fig. 23(b) and 23(d) in the case of KBC and AEH, however PBC shows the opposite trend. The bulk modulus (K) computed according to the elastic relations is very sensitive to Poisson's ratio (ν), as well as differences between the Young's modulus (E) and shear modulus (G) values, which are obtained from simulations, as can be seen in Fig. 23(b). The C-S-H gel formation between the particles creates a percolation network that can increasingly support the mechanical stresses in the microstructure as hydration proceeds. This translates into a corresponding increase in the moduli as shown in Figs. 23(a) and 23(c). Due to the increase in C-S-H gel volume fraction and simultaneous reduction in volume fraction of most of the other constituents, the microstructure tends to become more isotropic. A comparison of the elastic matrices obtained at various DOH indicates this trend as shown in Fig. 23(e). The effect of domain size on the elastic properties is shown in Fig.24 for cementitious domains of various sizes (8K, 125K and 1M). The effective properties (at constant DOH) asymptotically converge as the domain size becomes larger. Overall, the larger domains hydrate at a faster rate as compared with smaller domains having the same volume fractions of constituent phases (Fig.25). This may be due to an increase in the active reaction surface area with increasing domain volume. Hence for comparison purposes, the elastic properties of domains of various sizes need to be considered at equivalent DOH.

Fairly significant (between 35%-8%) differences between values of Young's modulus obtained by applying KBC and PBC to the microstructural domains are reported for cement by Smilauer [61] and for random composites by Kanit [47]. However, in the present study the difference was found to be smaller (<4%) and it does not follow the trend of elastic properties obtained from KBC being larger than those obtained from PBC. However the E and G values obtained by applying KBC and PBC are slightly lower than AEH estimates (Table 4).

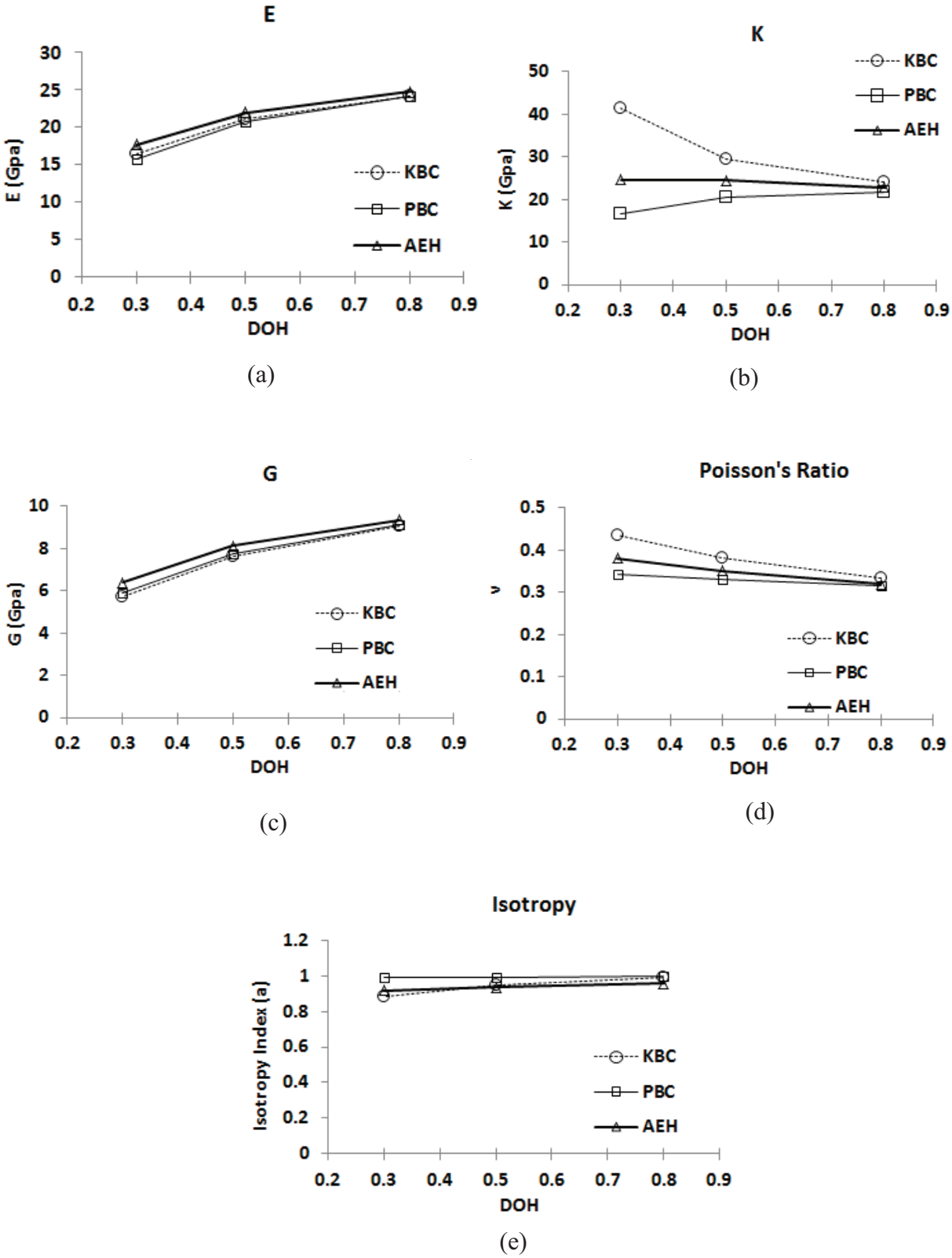

Figure 23. Effect of DOH on material bulk properties for 1M-RVE for KBC, PBC and AEH

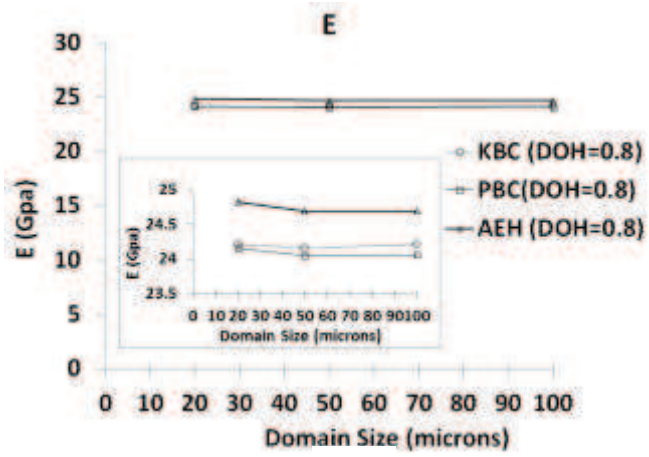

(a)

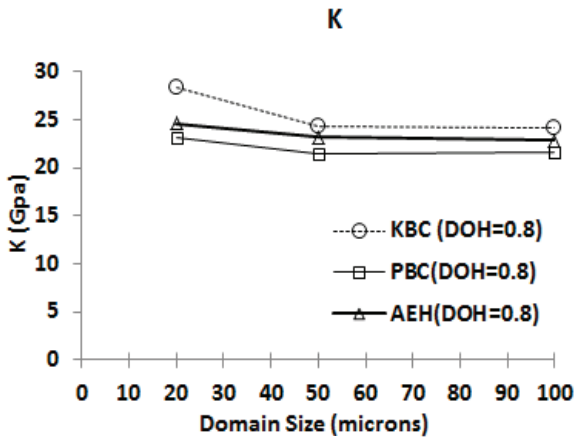

(b)

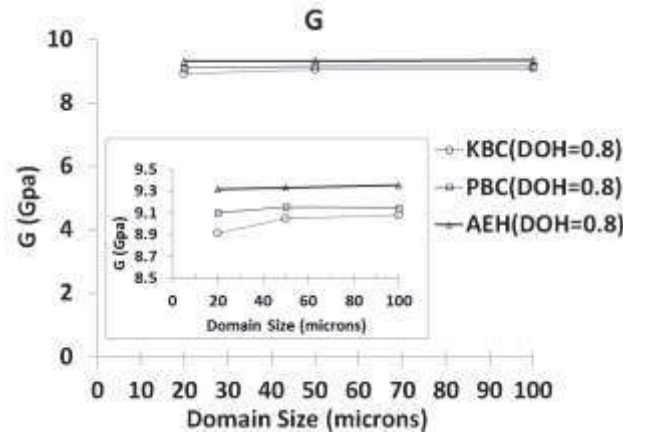

(c)

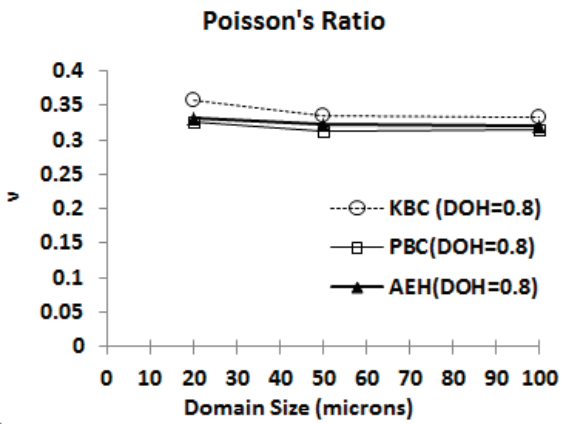

(d)

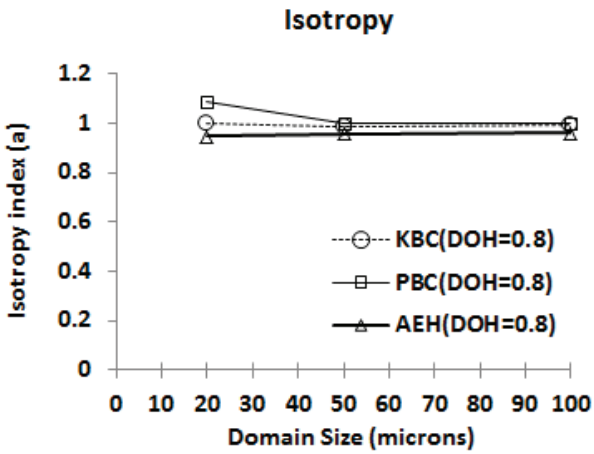

(e)

Figure 24. Effect of domain size on material bulk properties for DOH=0.8 for KBC, PBC and AEH

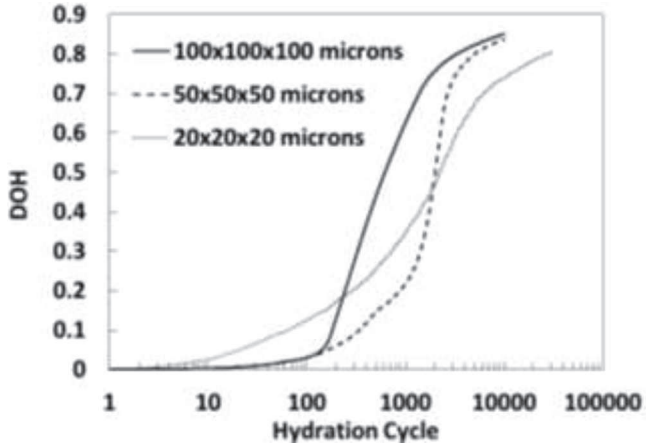

Figure 25. The effect of domain size on degree of hydration (α) (CEMHYD3D)

4.2.2. Windows

Windows ranging in size from 1K to 125K are extracted from a 1M-PMD (DOH=0.8) to qualitatively evaluate the local anisotropy within the larger domain. It is important to note that the particle distribution and volume fraction of each window is not consistent with that of the larger domain from which the window is extracted. The volume fractions of some of the major constituent phases that are contained within both the 1K and 8K windows are found to vary significantly (Fig. 26). Larger variation is observed in smaller windows. This variation is indicative of the local anisotropy in the volume of material contained within the larger 1M domain.

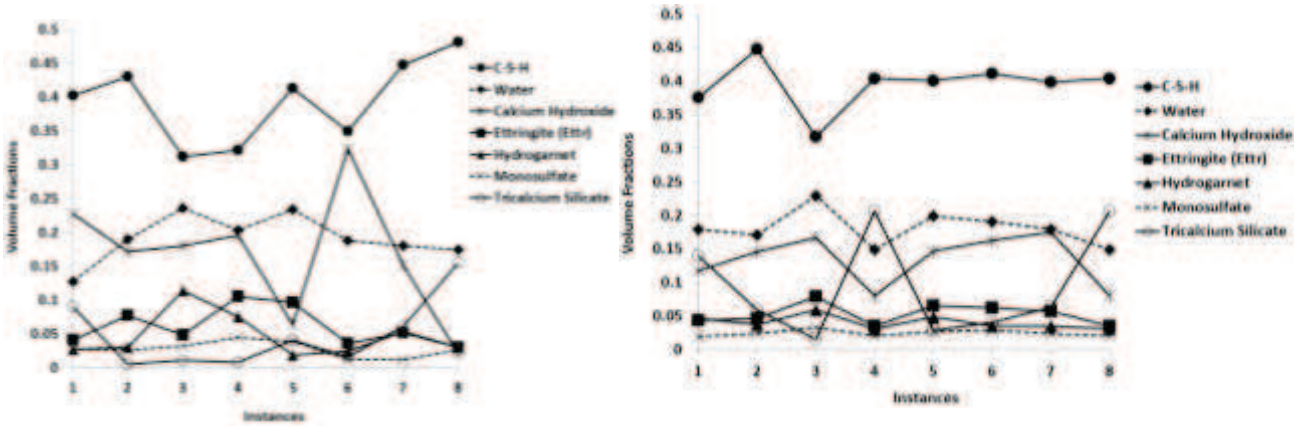

(a) (b)

Figure 26. Volume fractions of major phases for (a) 1K element and (b) 8K element windows

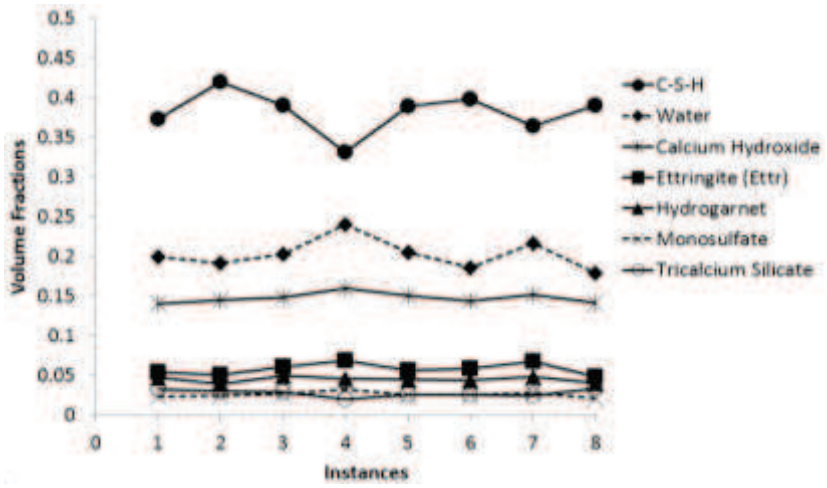

Figure 26-(c). Volume fractions of major phases for 125K element windows

Intuitively, as the window sizes become larger their average properties are expected to approach that of the bulk material. To evaluate the effects of domain size and random microstructure on the elastic properties, four 1M PMDs, each with different microstructure, are generated while maintaining the same PSD and volume fractions of the constituents. The resultant domain size is 200x200x100 (4M) finite elements.

Convergence studies are conducted on windows of various sizes (1K, 8K, 125K, 1M and 4M elements). For each case the average values obtained from 8 instances in the case of 1K, 8K and 125K windows; 5 instances of 1M and 1 instance of 4 M domains are reported. The convergence behavior of the elastic modulus (uniaxial deformation) normalized with respect to E_1 and G_{12} obtained from PBC applied to 4M- PMD is shown Figs. 27-28. Based on these numerical exercises, a 1M domain size seems to be the minimum required size such that computed properties are no longer sensitive to variations between random instances. This indicates that the 1M domain size is sufficient for an RVE to realistically represent the microstructure and effective bulk properties of the Type-I cement considered here. Though this exercise does not directly address the statistical aspects based on 2-way ANOVA or a t-Test, the results clearly show that both domain size and random microstructure do not significantly affect the elastic properties obtained from the domains of size equal to or larger than 1M elements.

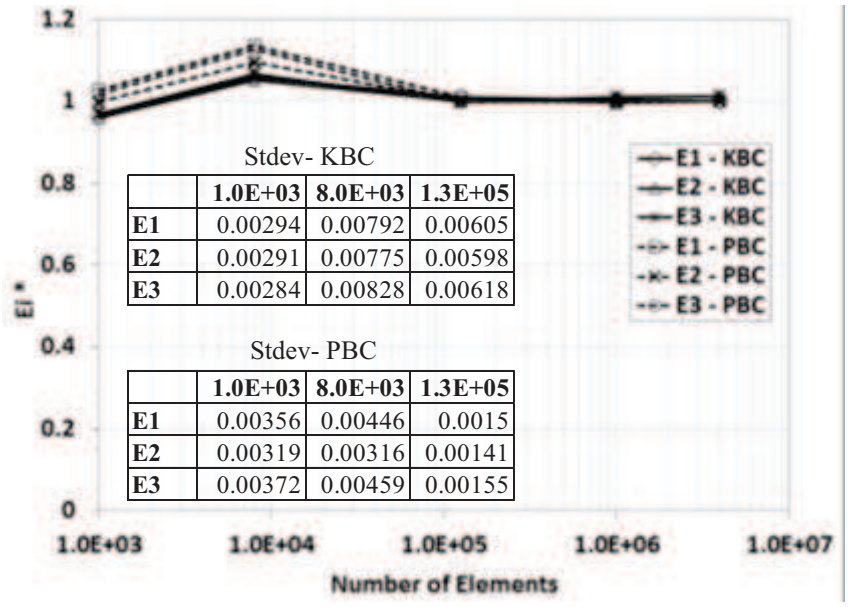

Stdev- KBC

	1.0E+03	8.0E+03	1.3E+05
E1	0.00294	0.00792	0.00605
E2	0.00291	0.00775	0.00598
E3	0.00284	0.00828	0.00618

Stdev- PBC

	1.0E+03	8.0E+03	1.3E+05
E1	0.00356	0.00446	0.0015
E2	0.00319	0.00316	0.00141
E3	0.00372	0.00459	0.00155

Figure 27. Elastic moduli (uniaxial) with increasing window size

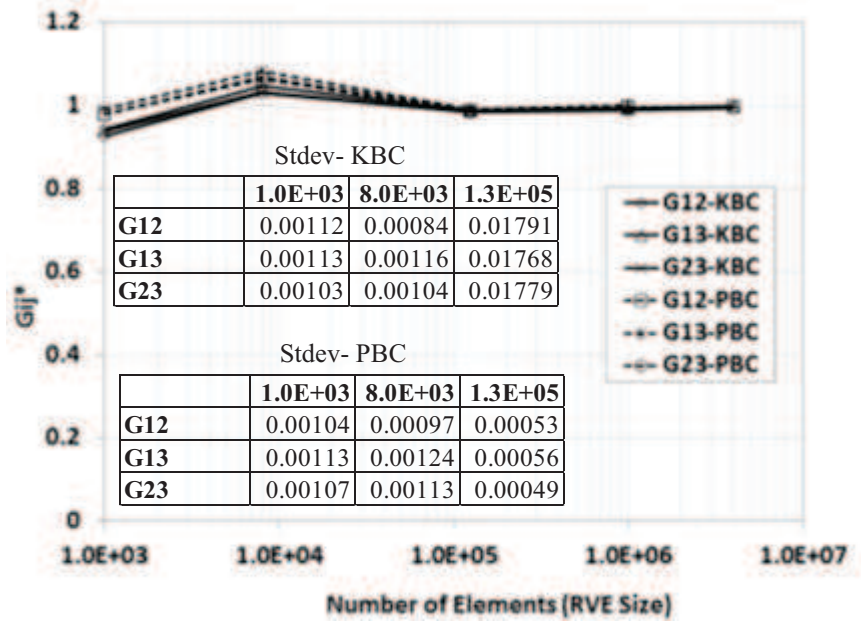

Stdev- KBC

	1.0E+03	8.0E+03	1.3E+05
G12	0.00112	0.00084	0.01791
G13	0.00113	0.00116	0.01768
G23	0.00103	0.00104	0.01779

Stdev- PBC

	1.0E+03	8.0E+03	1.3E+05
G12	0.00104	0.00097	0.00053
G13	0.00113	0.00124	0.00056
G23	0.00107	0.00113	0.00049

Figure 28. Elastic shear moduli G*ij* with increasing window size

4.3. Rule of Mixtures Based Homogenization

A rule of mixtures approach independent of the microstructure of the material is used to compute the effective bulk properties of the cementitious material. The theoretical extreme upper and lower bounds on effective material properties of multi-phase materials are the Voigt [62] and Reuss [63] bounds. The rule of mixtures based Voigt upper bound on the effective bulk (K*) and shear moduli (G*) of a mixture of n material phases is given by:

$$K^* = \sum_{i=1}^{n} f_i K_i \text{ and } G^* = \sum_{i=1}^{n} f_i G_i \tag{12}$$

The inverse rule of mixtures based Reuss lower bound on effective bulk (K*) and shear moduli (G*), is given by:

$$\frac{1}{K^*} = \sum_{i=1}^{n} \frac{f_i}{K_i} \text{ and } \frac{1}{G^*} = \sum_{i=1}^{n} \frac{f_i}{G_i} \tag{13}$$

Hashin (1962) [64] presented the composite (or coated) spheres model for determining the effective material properties for multi-phase materials, based on the dilute suspension model. Here a large number of uniformly distributed coated spherical inclusions that fill all space in a matrix are considered. The effective bulk modulus (K*) is given by:

$$\frac{K^*}{K_m} = 1 + 3(1-\nu_m)\sum_{i=1}^{n} \frac{\left(\frac{K_p^i}{K_m}-1\right)c_i}{2(1-2\nu_m)+(1+\nu_m)\left[\frac{K_p^i}{K_m}-\left(\frac{K_p^i}{K_m}-1\right)c\right]} \tag{14}$$

Where,

K_p^i=Bulk modulus of ith kind of inclusion,

K_m=Bulk modulus of matrix

K^* =Effective bulk modulus of heterogeneous material

ν_m=Poisson's ratio of matrix

c_i=volume concentration of ith kind of inclusion

$c = \sum_i^n c_i$ =volume concentration of inclusions

And the simplified formula for effective shear modulus (G*) is given by [64]:

$$\frac{G^*}{G_m} = 1 + 15(1-\nu_m)\sum_{i=1}^{n} \frac{\left(\frac{G_p^i}{G_m}-1\right)c_i}{7-5\nu_m+2(4-5\nu_m)\frac{G_p^i}{G_m}-2(4-5\nu_m)\left(\frac{G_p^i}{G_m}-1\right)c} \quad (15)$$

Where,

G_p^i=Bulk modulus of i[th] kind of particle, G_m=Bulk modulus of matrix

G^* =Effective bulk modulus of heterogeneous material

ν_m=Poisson's ratio of matrix

c_i=volume concentration of i[th] kind of particle

$$c = \sum_{i}^{n} c_i$$

For the upper bound, the effective bulk and shear moduli of the hydrated cement are obtained by assuming that the properties of the matrix are that of C-S-H. For the lower bound, the properties of the matrix are assumed to be that of water filled porosity (Table 1).The various theoretical bounds on the elastic moduli based on rule of mixtures are compared in Table 5 below:

Table 5. Comparison of theoretical bounds on homogenized elastic moduli for a 1M-RVE (DOH=0.8)

	Voigt (V)	**Reuss (R)**	**Hill**	**Hashin**
K(GPa)	26.33	9.02	17.68	25.78
G(GPa)	12.17	2.19e-4	6.09	11.59
Lambda	18.21	9.02	13.62	18.06
E (GPa)	31.32	6.58e-4	15.66	30.23
ν	0.30	0.50	0.40	0.30

The differences between Voigt and Reuss estimates are large when the phase moduli differ by more than a factor of two, producing poor estimates in the case of particulate composites. The large variation shown in Table 5 is consistent with the significant presence of porosity which has effectively zero Young's modulus. It is also observed that the Hashin estimates in this case are

close to the Voigt upper bound. In both these estimates the elastic properties are higher than those estimated by microstructure based homogenization (KBC, PBC and AEH).

The material properties predicted by the microstructure based methods for a 1M domain at DOH=0.8 are comparable to resonant ultrasound spectroscopy (RUS) based experimental data (Table 6) reported for a typical Type –I Portland cement with a w/c ratio of 0.40 [65]. In the current study, the Young's modulus (E) of the cement RVE is computed to be around 24.0 GPa, the Shear modulus (G) is around 9.0 GPa and effective Poisson's ratio (**ν**) is about 0.32 for a w/c ratio of 0.40. Similar but slightly different range of values for Young's modulus (20-25 GPa), Shear modulus (8-10 GPa) and Poisson's ratio (0.24-0.25) have been reported by several authors for Type-I cements with w/c ratio ranging from 0.4 to 0.5 [61, 66-68]. The authors believe that the reason for this difference is the variation in experimentally determined micro-scale material properties, different PSD, volume fractions of constituent phases and w/c ratios in cements studied at various research facilities.

Table 6. Experimental (RUS) results for hydrated cement paste with w/c=0.4 [65]

	C11	**C33**	**C12**	**C13**	**C44**	**ν**	**E**	**G**
(GPa)	24.23	--	6.69	--	8.77	0.216	21.55	8.8

4.4. Compressive strength of Hardened Cement Paste

Powers (1958) considered strength to be related to the concentration of solid hydration products in the paste and expressed this as a gel space ratio (X) defined by Eq.(17) below in which the gel pores are included in the gel volume [69]:

$$X = \frac{0.68\alpha}{0.32\alpha + \frac{w}{c}} \tag{17}$$

Where,

α = degree of hydration

w/c= water-cement ratio =0.40

The compressive strength (σ_c) is related to X by the equation:

$$\sigma_c = \sigma_O X(t)^n \tag{18}$$

where n=2.6 to 3.0 for typical cements.

In the case of the PMDs, the total porosity is taken as being equal to water porosity and volume of C-S-H is taken as total gel volume. Theoretical maximum strength is achieved when X=1, i.e., 100% hydration takes place. In literature several models are used to fit either degree of hydration or strength development vs time. A parabolic model developed by Knudsen and implemented in CEMHYD3D [70] provides a good fit to experimental data:

$$A = A_u \frac{k(t-t_0)^{1/2}}{1+k(t-t_0)^{1/2}} \tag{19}$$

Where, A_u = ultimate achievable value of the property = σ_O (compressive strength)

t0 = induction time which accounts for accelerated rate of hydration during the very early stage,

k = rate constant that is fitted to experimental data

The development of compressive strength for cementitious periodic domains of various sizes (8K, 125K and 1M) is plotted in Fig. 29. The trend in compressive strength development is similar to that of the degree of hydration. The development of the Young's modulus in the 1M-RVE, normalized to the modulus obtained from the 4-M PMD as a function of time (days) is shown in Fig. 30.

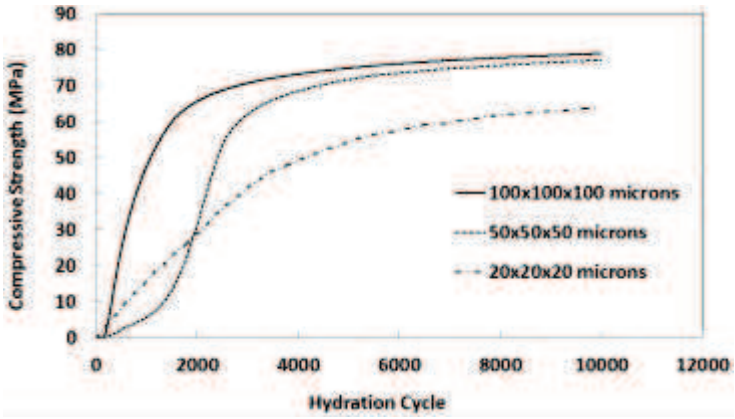

Figure 29. Development of the compressive strength (*f'c*) (CEMHYD3D)

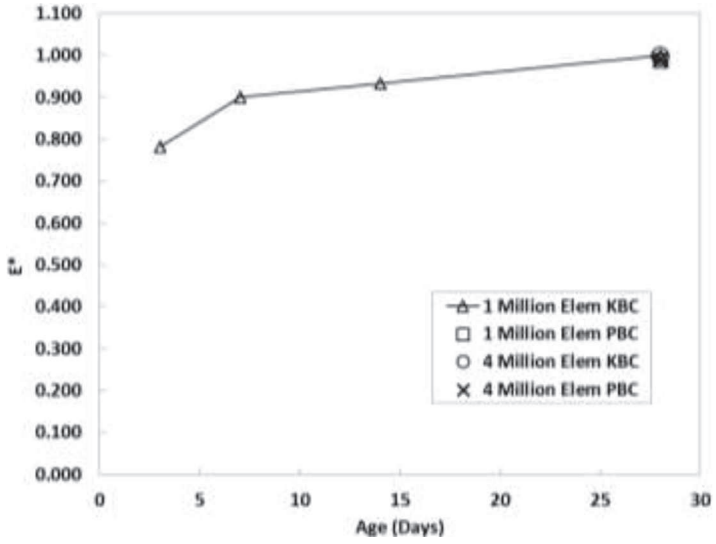

Figure 30. Development of the Young's Modulus (E) (ABAQUS)

4.5. Computational Resources

The computational resources of the Sequoia cluster at Mississippi Supercomputing Center (MCSR was leveraged. Sequoia is a 124 node cluster with 22 Altix XE 310, 24 Altix XE 320, and 78 Rackable computing nodes. Each Altix node consists of Dual Intel Xeon Quad-core E5420 Harpertown processors, a 1333 MHz Front Side Bus, a 12 MB L2 Cache, and a 250 GB Disk Drive. Each Harpertown processor consists of 4 2.5 GHz cores (or, effectively, CPUs) and 8 GB memory. 42 Altix nodes are configured with 16 GB memory each (2GB per core), but 4 Altix fat nodes are configured with 32 GB memory each (4GB per core). Each Rackable node has two six-core Intel Xeon X5650 (Westmere) processors, 36 GB of DDR3 RAM, a 2 TB internal SATA hard drive, and a QDR Infiniband network card. Overall, Sequoia has 3.44TB memory.

Table 7 Resource allocation on Sequoia at MCSR

RVE size (no. of elements)	**No. of Nodes**	**No. of CPUs/Node**	**RAM Allocation (Gb)**
1000	1	1	28
8000	1	1	28
1 Million	1	2	28
4 Million	4	1	140

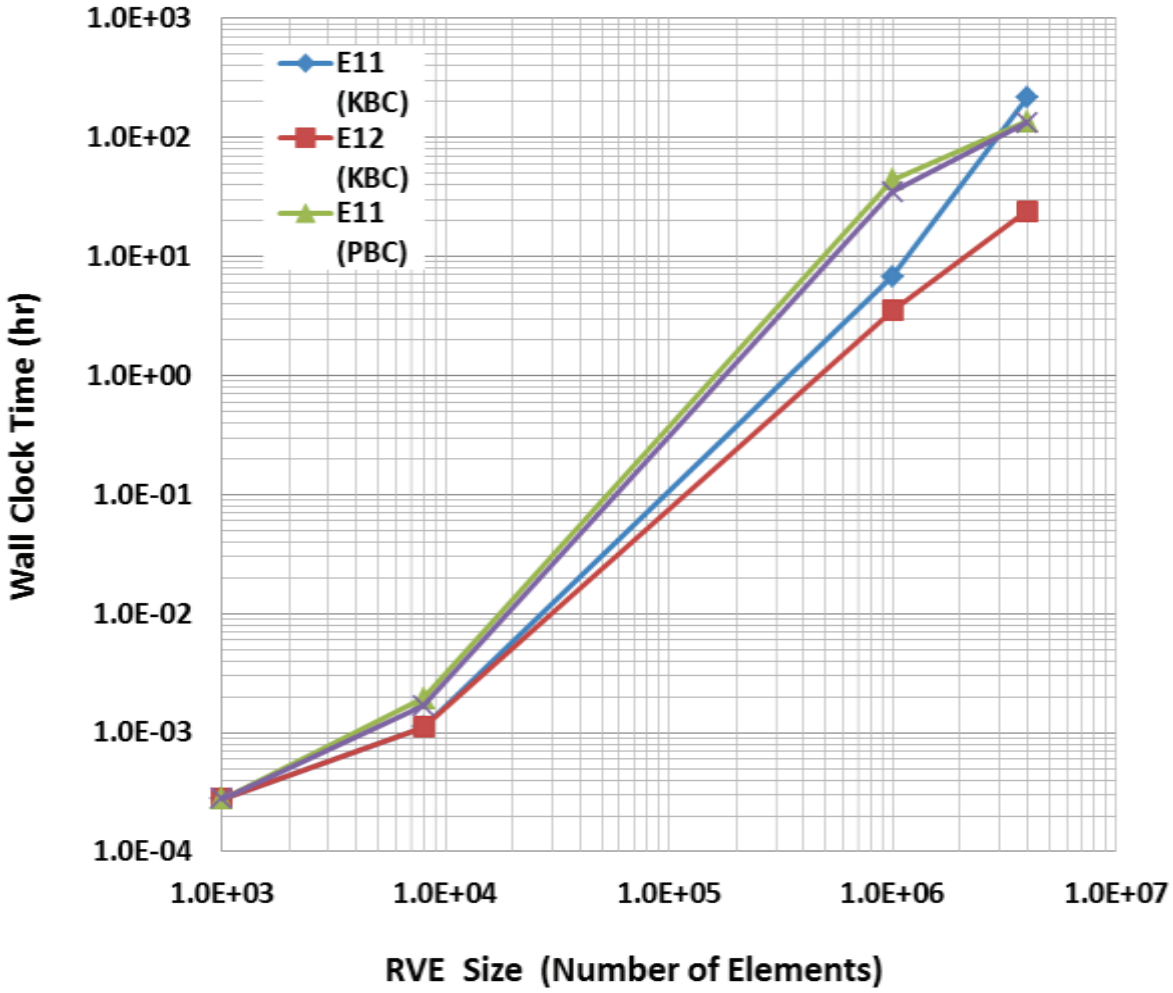

Figure 31. Wall clock time (hr) vs RVE size

CHAPTER 5

CONCLUSION AND FUTURE WORK

The results presented under this work clearly show how meso-scale effective properties can be determined using voxel based FEA approach. Analysis is conducted to obtain the elastic moduli and compressive strength of a Type-I cement paste. In this effort both KBC and PBC were investigated to determine if the elastic properties are invariant due to boundary conditions and results are compared with an alternate AEH methodology. In addition the method of "windowing" was used to access the randomness of the constituents and to validate how the isotropic elastic properties were determined. A comparison between the two domain sampling methods shows that windowing produces effective material properties with a larger variation than the PMD due to a higher variation in local phase volume fractions. Macroscopic properties obtained for various DOH and domain sizes, determined by applying KBC, PBC, AEH and rule of mixtures based homogenization are found to be comparable. It is shown that even though cement is a heterogeneous anisotropic material at the micro-level, the bulk properties are effectively isotropic.

Multiscale modeling (MM) is a computationally intensive approach that enables computation of elatic properties of heterogeneous cement with a wide variety of additives. Under a hierarchical MM approach, the individual properties of each constituent and additive material can be computationally determined using molecular dynamics (MD) simulations and this information can be passed on to the next level RVE based microstructural model. In future, this microscopic RVE based methodology will be further extended to investigate the effects of nano-scale additives on mechanical properties.

LIST OF REFERENCES

[1] Garboczi, E., and Bentz, D.P., 1996, Multi-scale Picture of Concrete and its Transport Properties: Introduction for Non-Cement Researchers, NISTR 5900, BFRL, NIST, Githesburg Maryland.

[2] Bernard, O., Ulm, F.J., and Lemarchand, E., 2003, "A multiscale micromechanics-hydration model for the early-age elastic properties of cement-based materials," *Cem. Concr. Res*., 33(9), pp. 1923-1309.

[3] Lee, J., Xi, Y., William, K., and Jung, C., 2009, "A multiscale model for modulus of elasticity of concrete at high temperatures," *Cem. Concr. Res*., 39(9), pp. 754-762.

[4] Wu, W., Al-Ostaz A., Cheng, A., and Chung S., 2010, "Concrete as a Hierarchal Structural Composite Material," *Int. J. Multiscale Comput. Eng.*, 6(5), pp. 585-595.

[5] Tennis, P.D. and Jennings, H.M., 2000,"A model for two types of calcium silicate hydrate in the microstructure of Portland cement pastes," *Cem. Concr. Res*., 30(6), pp. 855-863.

[6] Mondal,P., Shah,S.P.and Marks,L.D, ,2008, "Nanoscale characterization of cementitious materials," *ACI J. Mater.*, 105(2), pp. 174-179.

[7] Thomas, J.J. , Jennings, H.M. and Allen, A.J. , 1998 , "The surface area of cement paste as measured by neutron scattering: evidence for two c-s-h morphologies," *Cem. Concr. Res*., 28(6), pp. 897–905.

[8] Constantinides, G., Ulm, F.J. and Van Vliet, K., 2003,"On the use of nanoindentation for cementitious materials," *Mater. Struct.*, 36, pp. 191-196.

[9] Jennings, H.M., Thomas,J.J., Gevrenov,J.S., Constantinides, G., Ulm, F.,J, 2005, "Relating the nanostructure of concrete to engineering properties," 2nd Int. Symp. Nanotech. Constr., Bilbao, Spain.

[10] Haecker, C.J., Garboczi, E.J., Bullard, J.W., Bohn, R.B., Sun, Z., Shah, S.P., and Voigt, T., 2005, "Modeling the linear elastic properties of Portland cement paste," *Cem. Concr. Res*., 35(10), pp.1948–1960.

[11] Richardson, I. G., 2008, "The calcium silicate hydrates," *Cem. Concr. Res*., 38(2), pp. 137 – 158.

[12] Pellenq, R.J.-M. Lequeux, N., Vandamme, H.,2008, "Engineering the bonding scheme in C-S-H: the iono-covalent framework," *Cem. Concr. Res*., 38(2), pp. 159 -174.

[13] Richardson, I.G., 2000, "The nature of the hydration products in hardened cement pastes," *Cem. Concr. Compos.,* 22, pp. 97–113.

[14] Murray, S. J., 2009, "Determination of Strength and Stiffness of Calcium Silicate Hydrate using Molecular Dynamics," M.S Thesis, University of Arkansas.

[15] Lin, F., 2006, "Modeling of hydration kinetics and shrinkage of Portland cement paste," PhD. Dissertation, Columbia University.

[16] Smilauer V., 2005, “Elastic Properties of Hydrating Cement Paste Determined From Hydration Models,” Thesis. Czech Technical University in Prague.

[17] Allen, A.J., Thomas, J. J. and Jennings, H. M., 2007, “Composition and density of nanoscale calcium–silicate–hydrate in cement,” *Nature Mater.*, 6(4), pp. 311-316.

[18] Bentz, D.P. , Jensenb, O.M. Coats, A.M. Glasser, F.P. , 2000, “Influence of silica fume on diffusivity in cement-based materials I. Experimental and computer modeling studies on cement pastes,” *Cem. Concr. Res*., 30(6), pp. 953-962.

[19] Mei Qiang Chandler, J. F. Peters, and D. Pelessone, 2012, Modeling Nanoindentation of Calcium Silicate Hydrate, *J. Transp. Res. Board, No. 2142,* Transportation Research Board of the National Academies, Washington, D.C., 2010, pp. 67–74.

[20] J.J. Beaudoin,1 P. Gu, and R.E. Myers, “The Fracture Of C-S-H And C-S-H/Ch Mixtures,” *Cem. Concr. Res*., 28(3), pp. 341–347,1998.

[21] Jennings,H.M., Bullard,J.W., Thomas,J.J., Andrade, J.E., Chen, J.J. and Scherer,G.W., 2008, “Characterization and modeling of pores ans surfaces in cement paste: correlations to processing and properties,” *J. Adv. Conc. Tech.*, 6(1), pp. 5-29.

[22] Chandler, M.Q, Peters, J. F. and Pelessone, D., Modeling Nanomechanical Behavior of Calcium-Silicate-Hydrate, Final Report, ERDC/GSL TR-12-30, U.S. Army ERDC, Vicksburg, MS 39180.

[23] Moser, R.D., Allison, P.G., Chandler, M.Q., Investigation of High-Strain Rate Damage in Reactive Powder Concretes Using Instrumented Indentation Techniques, NICOM 4: 4th International Symposium on Nanotechnology in Construction.

[24] Sorelli,L., Constantinides, G., Ulm,F.J., Toutlemonde, F., 2008, “The nano-mechanical signature of Ultra High Performance Concrete by statistical nanoindentation techniques,” *Cem. Concr. Res*., 38(12), pp. 1447–1456.

[25] Dolado, J.S., and Breugel, K.V., 2011, “Recent advances in modeling for cementitious materials,” *Cem. Concr. Res*., 41(7), pp. 711–726.

[26] S. Kamali-Bernard,S., F. Bernard,F., Prince,W. , 2009, “Computer modelling of tritiated water diffusion test for cement based materials,” *J. Com. Mat. Sci.,* 45(2), pp. 528–535.

[27] H. A. Meier, E. Kuhl and P. Steinmann, 2008, “A note on the generation of periodic granular microstructures based on grain size distributions,” *Int. J. Numer. Anal. Meth. Geomech.* , 32(5), pp.509–522.

[28] Šmilauer,V. Hlaváček,P., Škvára, F., Šulc, R., Kopecký, L., Němeček, J., 2011, “Micromechanical multiscale model for alkali activation of fly ash and metakaolin,” *J. Mater. Sci.,*46 (20), pp 6545-6555.

[29] Andrade J. E., Fonseca and P. C., Jennings H. M.,2011, “A nanoscale numerical model of calcium silicate hydrate,” *Mech.Mater.*, 43(8), pp. 408-419.

[30] Shahsavari R., Pellenq R. J.-M., Ulm F. J., 2011, "Empirical force fields for complex hydrated Calcio Silicate layered Materials," *Phys. Chem. Chem. Phys.,* 13(3), pp. 1002-1011.

[31] Ulm F. J., Pellenq R. J.-M., Vandamme M., 2009, "Concrete: from atoms to concrete structures," Comp. Mod. Conc. Struct., Bicanic et al eds., Taylor and Francis Pub., pp. 69, 2010.

[32] Pellenq R. J.M., Kushima A., Shahsavari R. et al., 2009, "A realistic molecular model of cement hydrates," *Proc Natl Acad Sci U S A.*, 106(38), pp. 16102-16107.

[33] Smilauer,V., Krejci, T., 2009,"Multiscale Model for Temperature Distribution in Hydrating Concrete Multiscale Model for Temperature Distribution in Hydrating Concrete," *Int.J.Mult.Comp. Eng.,* 7(2), pp. 135-151.

[34] Maekawa,K., Ishida, T., and Kishi, T., 2003, "Multi-scale Modeling of Concrete Performance: Integrated Material and Structural Mechanics," *J. of Adv. Conc. Tech.*, 1(2), 91-126.

[35] Ye, G., van Breugel, K. and Fraaij, A.L.A., 2002, "Three-dimensional microstructure analysis of numerically simulated cementitious materials," *Cem. Concr. Res*., 33 (3), pp. 215-222.

[36] Princigallo, A., Lura, P., Levita, G. and van Breugel, K., 2003, "Early development of properties in a cement paste: A numerical and experimental study," *Cem. Concr. Res*., 33 (7), pp. 1013-1020.

[37] Grondin, F., Dumontet, H., Ben Hamida, A., Mounajed, G. , Boussa, H., 2007, "Multi-scales modelling for the behaviour of damaged concrete," *Cem. Concr. Res*., 37(10), pp. 1453–1462.

[38] Yeong, C. L. Y., and Torquato, S., 1998, "Reconstructing random media. II. Three-dimensional media from two-dimensional cuts," *Physical Review E,* 58(1), pp. 224-233.

[39] Bishnoi,S., 2008, "Vector Modelling of Hydrating Cement Microstructure and Kinetics," Doctoral Thesis No. 4606, École Polytechnique Fédérale De Lausanne, Suisse.

[40] Wu, W., Al-Ostaz,A., M., Cheng, A. H.-D.and Song, C. R. ,2011, "Computation of Elastic Properties of Portland Cement Using Molecular Dynamics," *J.Nanomech. Micromech.,* 1(2), pp. 84-90.

[41] Hill, R., 1963, ''Elastic Properties of Reinforced Solids: Some Theoretical Principles,'' J. Mech. Phys. Solids., 11, pp. 357–372.

[42] Hashin, Z., and Shtrikman, S., 1963, "A variational approach to the theory of elastic behavior of multiphase materials," *J. Mech. Phys. Solids*., 11, pp. 127–140.

[43] Willis, J., 1981, "Variational and related methods for the overall properties of composites," *Adv. Appl. Mech*., 21, pp.1–78.

[44] Nemat-Nasser, S., and Hori, M., 1999, "Micromechanics: Overall Properties of Heterogeneous Materials," 2nd ed. (Elsevier, Amsterdam).

[45]Sab, K., 1992, "On the homogenization and the simulation of random materials," *Eur. J. Mech. Solids*., 11, pp. 585–607.

[46] Huet, C., 1999, “Coupled size and boundary-condition effects in viscoelastic heterogeneous and composite Bodies,” *Mech. Mater.*, 31 (12), pp.787–829.

[47] Kanit, T., Forest, S., Galliet, I., Mounoury, V., and Jeulin, D., 2003, “Determination of the size of the representative volume element for random composites: statistical and numerical approach,” *Int. J. Solids Struct*., 40(13-14), pp. 3647-3679.

[48] Gitman, I.M., Askes, H., and Sluys, L.J., 2007, “Representative volume: Existence and size determination,” *Eng. Frac. Mech.*,74(16), pp. 2518-2534.

[49] Bentz, D.P., 2005, “CEMHYD3D: A three dimensional cement hydration and microstructure development package,” Version 3.0, NISTIR7232, US Dept. of Commerce.

[50] Bonen, D., and Diamond, S., 1991, "Application of Image Analysis to a Comparison of Ball Mill and High Pressure Roller Mill Ground Cement," in *Proc. 13th Int.Conf. Cem.Microscopy* , pp. 101.

[51] Bernard, F., Kamali-Bernard, S., and Prince,W., 2008, “3D multi-scale modeling of mechanical behaviour of sound and leached mortar,” *Cem. Concr. Res*., 38(4) pp. 449-458.

[52] Charmrova,R., 2010, “ Modelling and Measurement of Elastic Properties Of Hydrating Cement Paste”, Doctoral Thesis No. 4606, École Polytechnique Fédérale De Lausanne, Suisse.

[53] Kurkuri, S., 2005, “Homogenization of Damaged Concrete Meso-structures using Representative Volume Elements – Implementation and Application to Slang,” Masters Thesis, Inst. of Struct. Mech., Bauhaus–University Weimar, Germany.

[54] Ren, Z.Y., and Zheng, Q.S., 2002, “A Quantitative study of minimum sizes of representative volume elements of cubic polycrystals—numerical experiments,” *J. Mech. Phys. Solids.*, 50 (4), pp. 881-893.

[55] Šmilauer,V. and Bittnar, Z., 2004, “Effects of representative cube size on the simulation of Portland cement hydration in CEMHYD3D model, in: J.Walraven, J. Blaauwendraad, T. Scarpas, B. Snijder (Eds.),” 5th *Int.PhD Symp. Civil Eng.*, A. A. Balkema Pub., pp. 581–587.

[56] Hain,M., and Wrigers, P., 2005,“Simulating the Microstructure of cement based construction materials” Proc. of App. Math. Mech.,5, pp-401-402.

[57] Barbero,E.J., 2008, Finite Element Analysis of Composite Materials. CRC Press, 1st edition.

[58]Chung,P.W, Tamma,K.K, Namburu,.R.R., 2001, “Asymptotic expansion homogenization for heterogeneous media: computational issues and applications, *Composites Part A*, 32(9), pp-1291-1301.

[59] Ramsey,J.J., Chung,P.W., Unpublished article, Army Research Lab, Aberdeen Proving Ground, MD.

[60] Kanit,T., N’Guyen,F., Forest,S., Jeulin, D., Reed,M., Singleton,S., 2006, “Apparent and effective physical properties of heterogeneous materials: Representativity of samples of two materials from food industry,” *Comput. Methods Appl. Mech. Engrg.*, 195, pp.3960–3982.

[61] Šmilauer,V. and Bittnar, Z., 2006, "Microstructure-based micromechanical prediction of elastic properties in hydrating cement paste," *Cem. Concr. Res*., 36, pp. 1708–1718.

[62] Voigt, W., B.G. Teubner,1928, Lehrbuch der kristallphysik.

[63] Reuss,A., Angew,Z., 1929, "Berchung der fiessgrenze von mischkristallen auf grund der plastizit atsbedingung f¨ur einkristalle," *Math. Mech.*, 9, pp. 49–58.

[64] Hashin,Z., Elastic Moduli of Heterogeneous Materials, Technical Report No.9, Submitted to ONR, Contract No. 1866(02), Sept. 1960.

[65] W.Wu, A.Al-Ostaz, J.Gladden, A.H.-D.Cheng and G.Li, 2010, "Measurement of Mechanical Properties of Hydrated Cement Paste Using Resonant Ultrasound Spectroscopy," *Jnl. ASTM Int.*, 7(5).

[66] S. Kamali, M. Moranville, E.G. Garboczi, S. Pren, B. Grard, 2004, "Hydrate dissolution influence on the Young's modulus of cement paste," *Proc. Frac. Mech. of Conc. Strs*., Li, et al., (Eds.), Vail.

[67] C.-J. Haeckerd, E.J. Garboczia, J.W. Bullarda, R.B. Bohnb, Z. Sunc, S.P. Shahc, T. Voigt, 2005, "Modeling the linear elastic properties of Portland cement paste," *Cem. Concr. Res*., 35, pp. 1948 – 1960

[68] L. Lam, Y.L. Wong, C.S. Poon, 2000, "Degree of hydration and gel/space ratio of high-volume flyash/cement systems," *Cem. Concr. Res*., 30, pp.747-756

[69] Bentz, D.P., 1997, "Three-Dimensional Computer Simulation of Portland Cement Hydration and Microstructure Development," *J. Am. Ceram. Soc.*, 80(1), pp. 3-21.

APPENDIX

Instruction of ABAQUS job submission in supercomputers at The University of Mississippi (MCSR)

First, we need to open the "SSH Sequia File Transfer Client Software" which can be downloaded from the following webpage:

https://shareware.unc.edu/

Then, we need to click on “quick connect”. In the “Connect to Remote Host pop-up window”, we need to enter:

Hostname: hpcwoods.olemiss.edu

User Name: *********

Password: **********

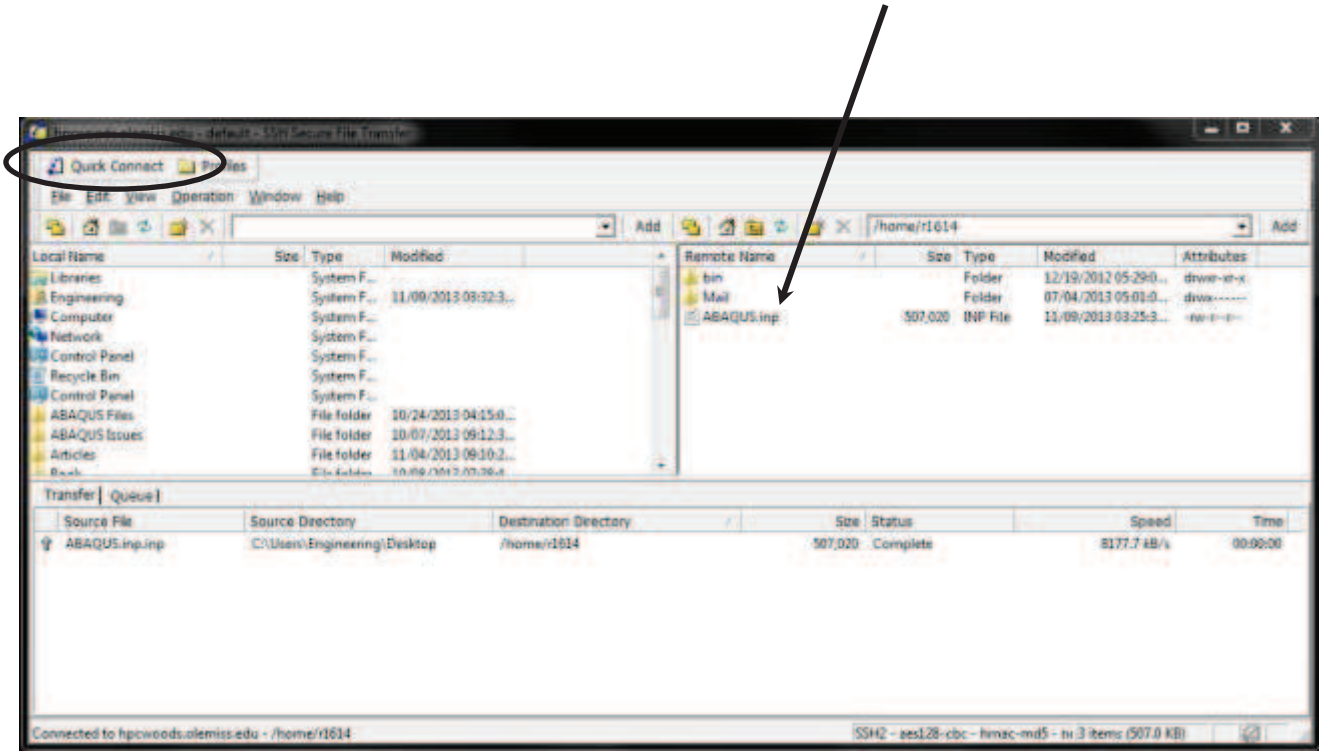

ABAQUS inp file should be copied and pasted in the place which is shown in the above picture. Now, we need to open the “SSH Secure Shell”

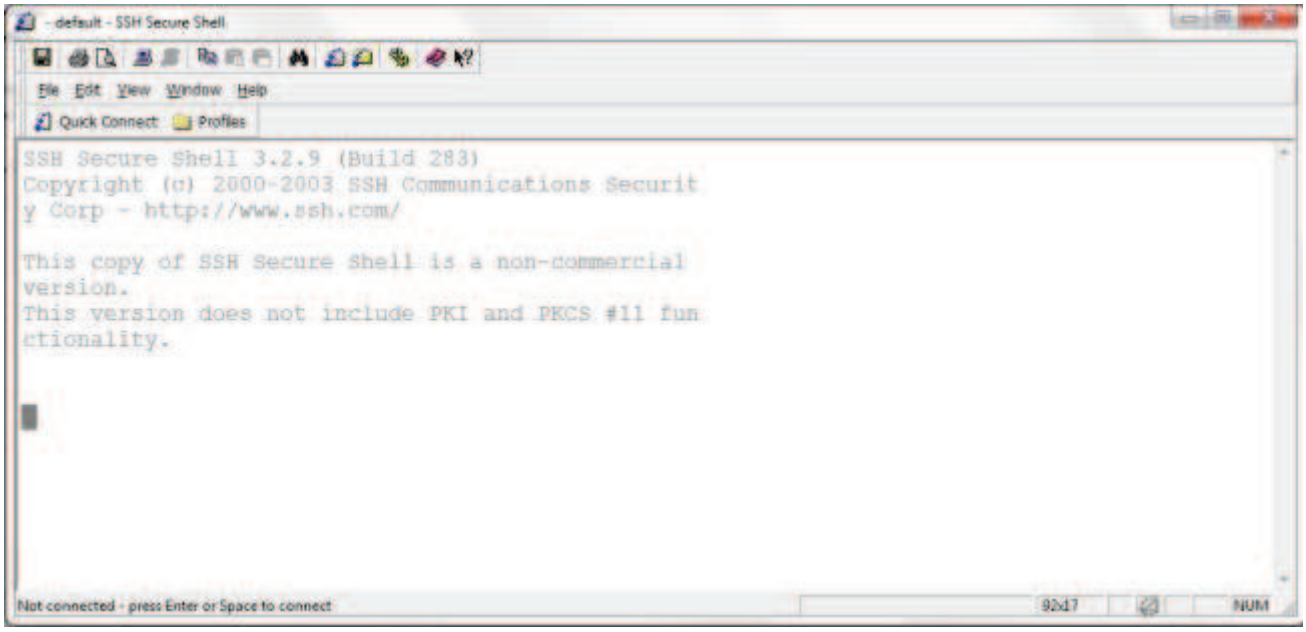

Here, a *.inp file can be transferred into the "Sequoia Environment". Again, we need to click on quick connect. After entering the hostname, username and password in pop-up windows, following commands should be inserted step by step.

1- ls (in order to see the list of files)

2- scp filename.inp sequoia:~ (in order to transfer the *.inp file into sequoia)

3- ls –l (in order to see the list of files)

4- chmod 600 Filename.inp (for the purpose of security)

5. ssh Sequoia (in order to enter to sequoia environment)

In the new appeared window, we need to insert the following commands as well.

6. ls

7. chmod 600 *.inp

8. mkdir directory (in order to make directory)

9. mv filename.inp directory (in order to move the file to that directory)

10. cd directory (in order to work only on the files in that directory)

11. ls –l

12. cp ~/abaqus.pbs Filename.pbs (in order to create a ABAQUS script)

13. nano Filename.pbs (in order to open the ABAQUS pbs script job)

Here, time needed to run a job and memory space can be allocated in ABAQUS pbs script. One recommended sample of ABAQUS script is as follows:

```
"
#!/bin/csh
#PBS -N Filename
#PBS -j oe
#PBS -l nodes=1:ppn=2
#PBS -l mem=28000mb
#PBS -l walltime=66:00:00
cd $PBS_O_WORKDIR
setenv SCRDIR /tmp/$PBS_JOBID
mkdir -p $SCRDIR
/usr/local/apps/abaqus/Commands/abq6102 job=Filename input=Filename.inp \
"
```

Now, we need to press "Ctrl+O" to save the changes and press "Ctrl+x" to exit.

14. ls

15. qsub Filename.pbs (in order to run the job)

16. qstat number (number is that produced in by command 15)

17. qstat -f number (number is that produced in by command 15)

18. qstat -u username (in order to see the status of jobs by the user)

To get the results, we need to enter the following commands:

19. cd directory/

20. ls

21. scp Filename.odb hpcwoods:~

At this moment the Filename.odb is in hpcwoods environment and it can be transferred to the system of the user.

VITA

Mohammadmehdi Shahzamanian Sichani (Medi) was born on 26 of April in 1984 in one of the historical city of Iran by the name of Isfahan.

He got started studying mechanical engineering in September of 2002 in the field of solid mechanics at Shahid Bahonar University of Kerman,Iran. Also, he has been student exchange in Isfahan University of Technology (IUT) for three semesters during his BS study.

From June of 2008 to 2010 he was MSc student of Mechanical and Manufacturing Engineering Department in Universiti Putra Malaysia (UPM) emphasized on mechanical structures. He has worked on functionally graded materials (FGMs) and their applications in brake disk. Medi is now the author of some journal and conference papers related to the functionally graded (FG) brake disk.

In August of 2011, he continues his study as a graduate student in the Department of Mechanical Engineering at The University of Mississippi in the field of material mechanical behavior especially brittle materials under advisory of Dr. Arunachalam Rajendran. This MS thesis is a part of his Ph.D. program. Furthermore, two conference papers and one journal papers related to this thesis has been published.